Spring 5-15-2020

CFD Analysis of a Wind Turbine Airfoil with Flap

heyou tan
Washington University in St. Louis

WASHINGTON UNIVERSITY IN ST. LOUIS

School of Engineering and Applied Science

Department of Mechanical Engineering and Material Science

Thesis Examination Committee:

Ramesh Agarwal, Chair

David Peters

Swami Karunamoorthy

CFD Analysis of a Wind Turbine Airfoil with Flap

By

Heyou Tan

A thesis presented to

McKelvey School of Engineering of Washington University in St. Louis in partial fulfillment of the requirements for the degree of Master of Science

May 2020

St. Louis, Missouri

Table of Contents

List of Tables

List of Figures

Acknowledgements

First of all, I would like to thank to Dr. Ramesh K. Agarwal for his guidance and instructions on this research. I have learned not only about knowledge in aerodynamics and computation fluid dynamics, but also the capacity about how to generate mesh and the implementation of Fluent and remain persistent in research.

I would like to acknowledge my committee members, Dr. Peters and Dr. Karunarmoorthy, for taking the time to read the thesis and attend its defense. Thanks to Xiang Zhang for helping me on complex mesh generation. Thanks to Gongyu Tang for his guidance in doing analysis of multi-element airfoil. Finally, I really appreciate all my colleagues in CFD lab for their continuous help and encouragement.

Heyou Tan

Washington University in St. Louis

May 2020

Dedicated to my parents.

I would like to dedicate this thesis to my father (Shiming Tan), my mother (Huijun Guo) for their unconditional support.

I will never succeed without their guidance, influence and encouragement.

ABSTRACT

CFD Analysis of a Wind Turbine Airfoil with Flap

By

Heyou Tan

Master of Science in Area of Study

Washington University in St. Louis, 2020

Research Advisor: Professor Ramesh K. Agarwal

The focus of this thesis is to evaluate the aerodynamic performance of NREL S809 airfoil (widely used airfoil for wind turbine blades) with a trailing-edge flap by numerical simulations. In the simulations, the geometry of the flap and the gap between the main element and the flap are varied. The airfoil geometry is created in Design Modeler and structured mesh around the airfoil is generated using meshing software ICEM. Simulations are performed using the Reynolds-Averaged Navier-Stokes (RANS) equations with SST k-ω, Spalart-Allmaras (SA) and Wray-Agarwal (WA) turbulence models at Reynolds number 10^6 at angles of attack of 0^o, 5^o, 10^o, 15^o, and 20^o. First, numerical solutions are validated against the experimental data for S809 airfoil without flap. Then the numerical simulations are conducted with a Gurney flap at various angles of attack. The lift coefficient and the drag coefficient are calculated and are compared with S809 plain flap to and Gurney flap to evaluate the effect of flap on the airfoil performance. The velocity and pressure contours are plotted and compared for airfoil within three turbulence models on two different types of flaps to analyze the details of the flow field and pressure distribution. Computed results show that the presence of trailing-edge Gurney flap provides higher lift and lift-to-drag ratio compared to original airfoil demonstrating its promise for larger wind energy extraction.

Chapter 1: Introduction

This chapter provides the background of the wind energy demand and methods used to improve aerodynamics performance, the scope and strategy of this thesis is also included.

1.1 Motivation

As tremendous energy demand from cross-world industrials and facilities increases, new type of energy replacement has been on stage of environmental preservation issues. Among renewable energy categories, wind energy has obtained advantages of free-use, controllable, unlimited by regions and weather, and massive capacity factor. According to Wind Technologies Market Report [1] in 2017 by the U.S. Department of Energy (DOE), wind power has reached a peak point of 7,017MW working load added in the United States with a $11 billion investment.

Technically, it is of great importance to improve wind power coefficient, contributing effective engineering output, and this can be addressed by wind blade optimization, which converts more energy on the airfoil of blades. Horizontal-axis-wind-turbines (HAWTs), are one of the two industrial-applied axis wind turbines, generate power as a linear correlation with lift coefficient(Cl) over drag coefficient(Cd), hence, the ratio of Cl/Cd is a significant parameter of increasing aerodynamics performance.

1.2 Scope of the Thesis

One of the goals in this thesis is to figure out coefficient improvements deploying flap at trailing-edge of an airfoil. Recent study has shown that there are enhanced investigations upon large-scale blade designs for wind turbines, of which target is to decrease quantities of wind towers and power

cost, by augmenting lift coefficient and lift-to-drag-ratio [2]. And this approach would be satisfied by the installation of various types of rotatable flaps.

It also presents experimental analysis of a trailing-edge flap under variable angles of attack and flap deflection angles and the effect of vortex generation due to adverse pressure gradient and larger flap deflection angle. The NREL S809 laminar-flow airfoil, obtains a chord length of 1000mm and thickness of 21%, is an ideal proscribed model for HAWTs [3][4]. Flow field is setup as default in FLUENT, and wind velocity is derived from IEC Wind Class 1 datasheet, airfoil is subjected in low Mach number flow, which is considered as incompressible flow, corresponding to one million of the Reynolds numbers. Commercial computational fluid dynamic software ANSYS FLUENT is applied in this paper and entire aerodynamic data is predicted by solving Reynolds-Averaged Navier-Stokes (RANS) equations at angles of attacks from 0 to 20 degrees and flap deflection angles from -5 to 10 degrees. The results meet the agreement with a growth of lift coefficient, drag coefficient and Cl/Cd ratio, in addition to vortex on the upper surface is remarkably eliminated by the introduce of trailing-edge flap.

Chapter 2: Methodology

2.1 Physical Model

According to a paper by Douvi and Margaris [5], a comparison between aerodynamic performance of NACA 0012 and NREL S809 wind turbine airfoil has been conducted, and it was concluded that latter operates at a superior level, the turbulence model selection would also be discussed in the thesis. Because of the assets of S809, it is selected, previous experimental data also showed that there is only laminar flow over the forward half of the surface when angle of attack is below 5°, backward half airfoil endures laminar separation due to turbulent reattachment [6]. As angle of attack is increased further, separation region moves towards leading-edge, and finally stall is taken place at approximately 20°.

The length of airfoil chord is setup as 1000mm. Barlas [7] indicated that a 10% overall chord length trailing-edge flap obtained a good control of aerodynamic load fluctuations, utilizing a flap deflection angle range from -5 to 10°. Unsteady fluctuations on blades considerately affect the lifetime and reliability of wind turbine system [8], therefore, flap deflection angle and flap gap should be taken into account when designing a physical model. The flap gap distance is set to 1mm, where greater difference provides lower aerodynamics performance. Figure 1.1 displays the schematic of general physical geometry

Table 2.1: Chord and Flap Settings

	S809 airfoil
Chord length	1000 mm
Max thickness	210 mm
Length of flap	100 mm
Angel of attack	0 - 20 deg.
Flap Deflection	-5 - 10 deg.

Flap Gap	1 mm

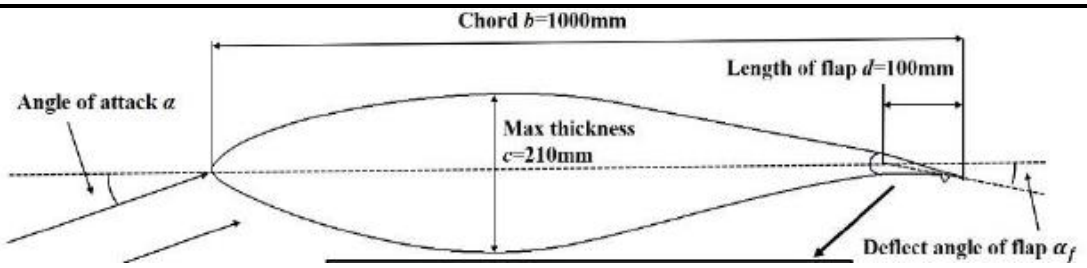

Figure 1.1 Modeling of S809 airfoil with trailing-edge flap

2.2 CFD Simulation

2.2.1 Simulation Method

The commercial CFD software ANSYS FLUENT 19.2 is employed in the simulations. The steady compressible Reynolds-Averaged Navier-Stokes (RANS) equations are solved using the finite volume method with SST K-ω, Spalart-Allmaras and Wray-Agarwal turbulence models. The SST k-ω turbulence model is a two-equation eddy viscosity model combing the best characteristics of the k-w and k-ε turbulence models. The Spalart-Allmaras turbulence model is the most commonly used one-equation eddy-viscosity turbulence model. All computations are performed in double precision. A second order upwind scheme is utilized for the convection terms and a second order central difference scheme is used for the diffusion terms. The SIMPLE algorithm is employed for the pressure-velocity coupling. Menter [9] developed the shear-stress transport (SST) k–ω model and it is advantageous of more accurate and reliable when separation flows occur under adverse pressure gradient, where the phenomenon is likely to appear in turbulence flow. Consequently, the specific turbulence model is selected, in the meantime, since the flow is considered at incompressible, there is no energy equation added into the system. The Wray-Agarwal model is a one-equation eddy-viscosity model derived from k-ω closure. Like the SST k-ω model, it behaves like k-ω model near the wall behavior and like k-ε model in free-stream. It has been applied to

several canonical cases [10] and has shown improved accuracy over the SA model and competitiveness with the SST *k-ω* model for wall bounded flows with small regions of separation The implementation of WA model is operated with UDF file named "Wray-Agarwal 2017m" version and has been extended to Wall-Distance-Free (WDF) version and to *transitional* flows (WA-γ) by including the intermittency equation

2.2.2 Boundary Conditions

For airfoil in the unbounded flow, the inlet, outlet boundaries are located 40c away from the airfoil. Standard air parameters include environmental temperature = 273.15K, air density is ρ = 1.225 kg. m^{-3} and the viscosity is μ = 1.7894e-5 kg. m. s^{-1}. Subsequently, inlet velocity is set to 15m/s, known as the free stream velocity, outlet gauge pressure defaults as 0 pascal, and these are regarding to Reynolds number reaches 10^6. Angle of attack varies the velocity inlet components with X and Y velocity (X-velocity is set to cosine angle of attack and Y-velocity is set to sine angle of attack). The author studies AoA ranging from 0 to 10 in this research and the airfoil is set as a no-slip stationary wall.

2.3 Governing Equations

Thanks to the low Reynolds number of the wind turbine, the flow field near the airfoil and flap can be considered as an incompressible viscous fluid. The solution is based on the incompressible Reynolds averaged Navier–Stokes (RANS) equations, which can be written as

$$\frac{\partial U_i}{\partial t}+\frac{\partial\left(U_i U_j\right)}{\partial x_j}=-\frac{1}{\rho_0}\frac{\partial P}{\partial x_i}+\nu\frac{\partial^2 U_i}{\partial x_j^2}+f_i \qquad (1)$$

$$\frac{\partial U_i}{\partial x_i}=0 \qquad (2)$$

where *Ui* is velocity; P is incompressible pressure, ρ is density, ν is kinematic viscosity, and fi is the added body forces. The expression and values of those variables are provided in Ref.[11].

The incompressible pressure coefficient can be written as follows:

$$Presure\ Coefficient = 1 - \left(\frac{U}{U_\infty}\right)^2$$

U is inlet velocity and U_∞ is far field velocity, and the maximum possible value of the Cp at the stagnation point in incompressible flow is 1. For dimensional analysis, Cp depends on Mach number, Reynolds number, shape, orientation of body and location on body

The lift coefficient relates the *AOA* to the lift force and can be calculated from:

$$Lift\ Coefficient = \frac{2L}{\rho_\infty {U_\infty}^2 A}$$

where L is lift force, ρ is density , U is velocity and A is airfoil area. The lift coefficient also contains the complex dependencies of object shape on lift

The drag coefficient is value of the effectiveness of a streamline aerodynamic body shape in reducing the air resistance to the forward motion, which described as

$$Drag\ Coefficient = \frac{D}{\rho_\infty {U_\infty}^2 A/2}$$

It contains not only the complex dependencies of object shape and inclination, but also the effects of air viscosity and compressibility. But the compressibility effects are negligible at low speeds

2.4 Mesh Generation

In the meshing process, a C-H domain is selected with 20 times of chord length from inlet boundary to airfoil and the same distance along to the outlet boundary. After calculation of mesh independent study, 150,000 quadrilateral cells are conducted to achieve accurate numerical solutions. Results from ICEM illustrated a first boundary layer thickness of 2.3e-5m and a Y Plus value of 1in Fig 2.1. Orthogonal quality is a mesh quality method, which tests out the first layer cell angle perpendicular to the prescribed surface and this method is applied, gives average orthogonal

quality 0.96 in Fig 2.2(a). In addition, author used another mesh quality method named aspect ratio to provide further refinement of grid controls, Fig 2.2(b) represents the average number of aspect ratio is 1.26 of the refined grids. Both of the quality approaches are within a reasonable range and afford experimental accuracy for numerical solutions.

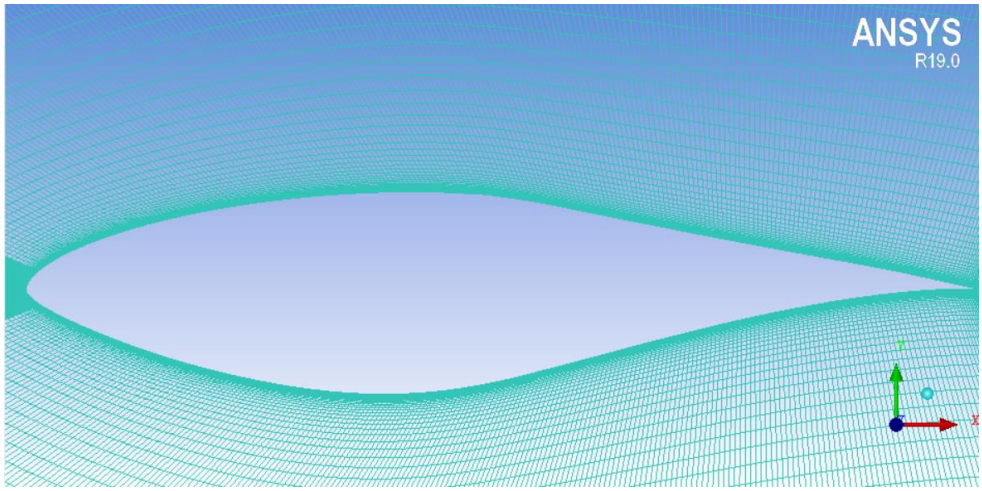

Fig 2.1 Computational structured grids

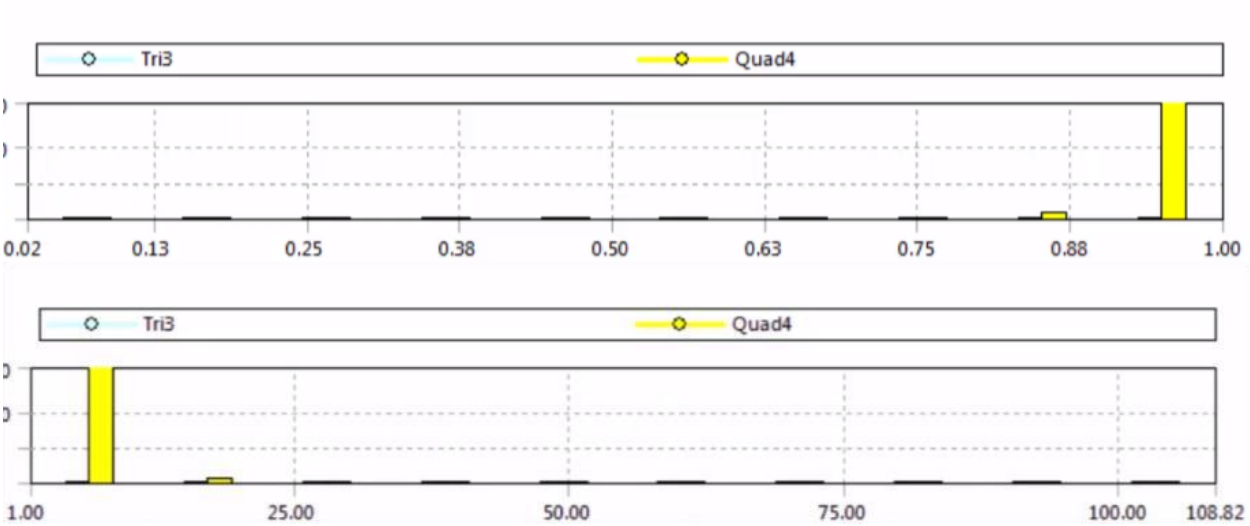

Fig 2.2(a) Orthogonal quality; Fig 2.2(b) Aspect ratio quality

2.5 Validation of the Solution Methodology

The validation case of was conducted for commercial solver, ANSYS Fluent. Experiment data of Bofeng et al. [8] is used to validate the numerical solution methodology. Fig 2.3 shows the comparison between calculated data from CFD and experimental data for S809 airfoil and a range

of angle of attack -5 degree to 25 degree is subjected to X-axis coordinate, coupling with a Y-axis coordinate of lift coefficient and drag coefficient. It is clearly to observe that two curves perfectly meet agreement before 17.5 degree, as stall occurs when angle of attack continues to increase. Besides, stall phenomena act that the calculated lift coefficient data is slightly greater than experimental data and CFD drag coefficient data is smaller than that from experimental data. And this also could due to various boundary conditions and initial predictions. In summary, this calculation validates the numerical approach employed.

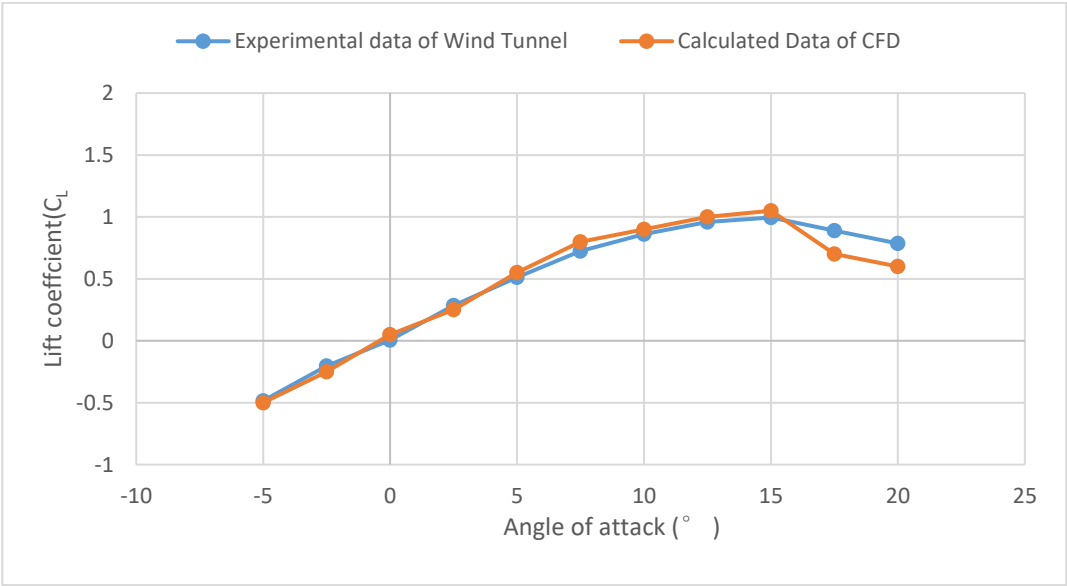

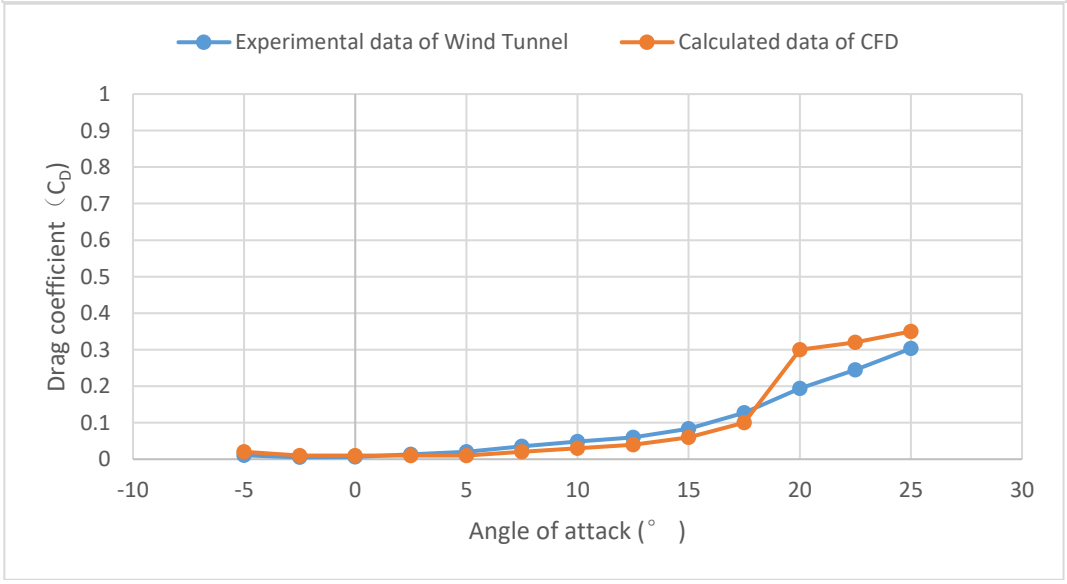

Fig 2.3 Lift and Drag coefficient of S809 airfoil

Chapter 3: S809 Airfoil with Plain Flap Simulation

3.1 Flow Field Information and Discussion

According to the previous validation test, aerodynamics characteristics can be significantly influenced by angle of attack, near the airfoil tip. Since there is a non-stall to stall angle of attack range, included 0, 5, 10, 15 and 20 degree, these angles are selected and compared. Flap deflection angle is 2.5 degree in this scenario in order to set up simplex variable, and all other parameters are identical as boundary conditions implemented by three different eddy-viscosity turbulence models.

3.1.1 Behaviors under Spalart-Allmaras (SA) One-Equation Model

Fig 3.1 shows the velocity contours under five angles of attack, it can be seen that there is a decreasing velocity gradient on the lower surface as AoA is increasing(stagnation point is clearer to see). The maximum velocity is also increasing at the leading edge when degree goes up, until it stops at 20 degrees. Another finding is the separation region starts to expand as AoA is over 10 degrees, where stall is occurred, and it is continuous to enlarge and completely cover the upper surface.

Fig 3.2 displays the pressure coefficient contours: as the developing angles, lower surface generates bigger pressure, causes higher lift force, while the maximum lift power places at 15 degrees angel of attack and decreasing afterwards. Besides that, due to plain flap introduction, there is also a rising pressure difference near the rear edge, however it is not obvious at the initial AoA condition. Plus, some anomalous pressure jump region located at high angle ranges, where it can be explained by the flow separation.

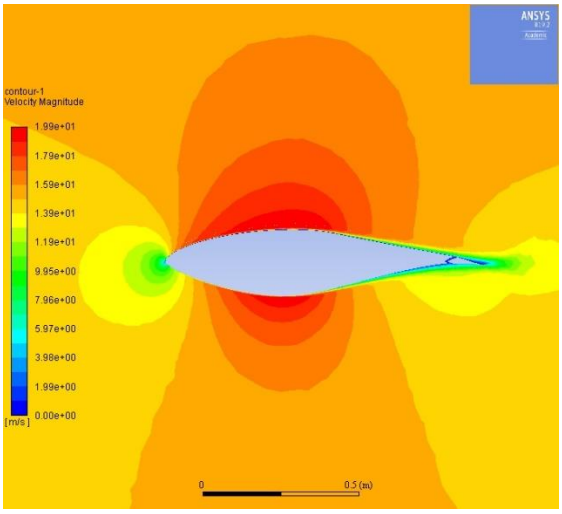

Angle of attack = 0 degree

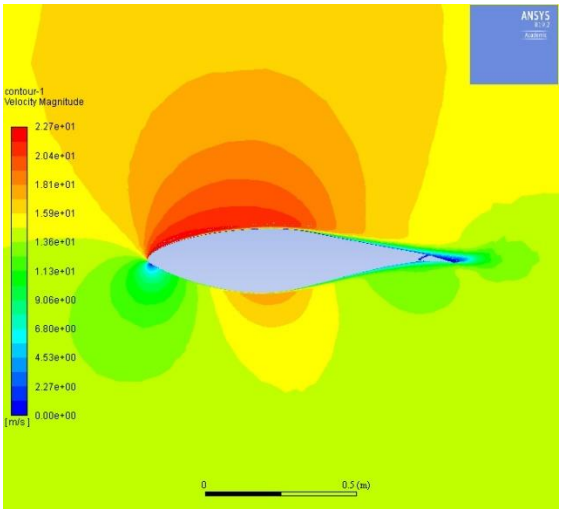

Angle of attack = 5 degrees

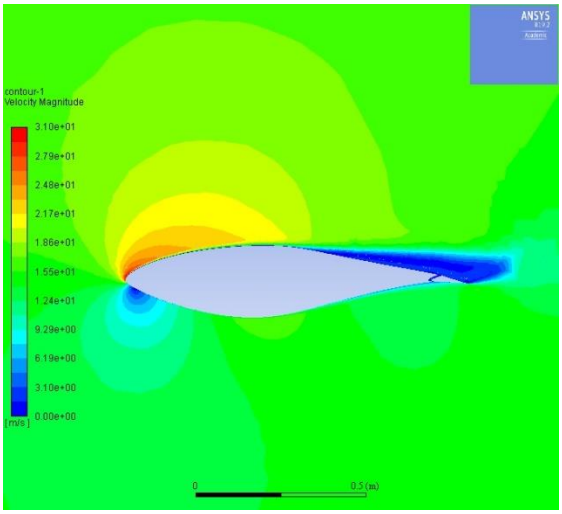

Angle of attack = 10 degrees

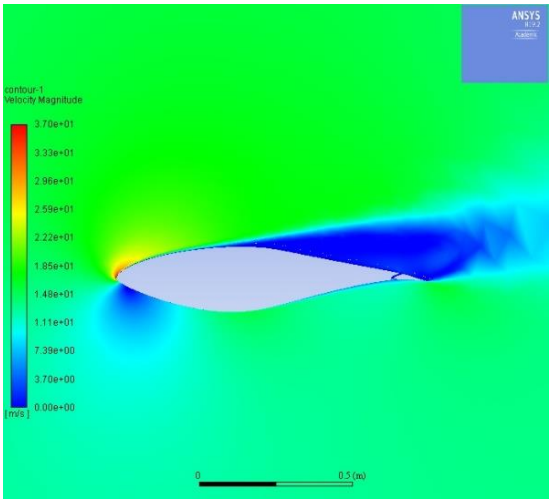

Angle of attack = 15 degrees

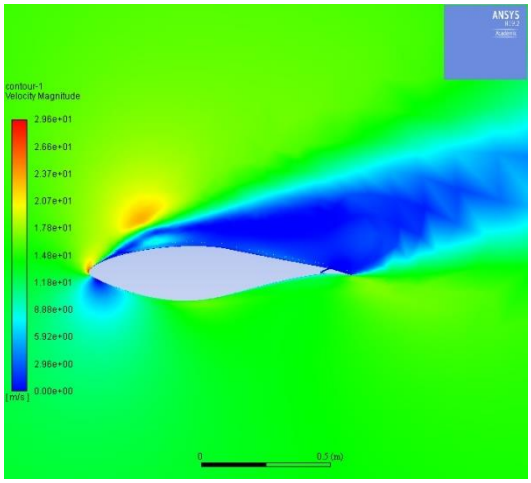

Angle of attack = 20 degrees

Figure 3.1 Velocity contours at plain flap in SA model

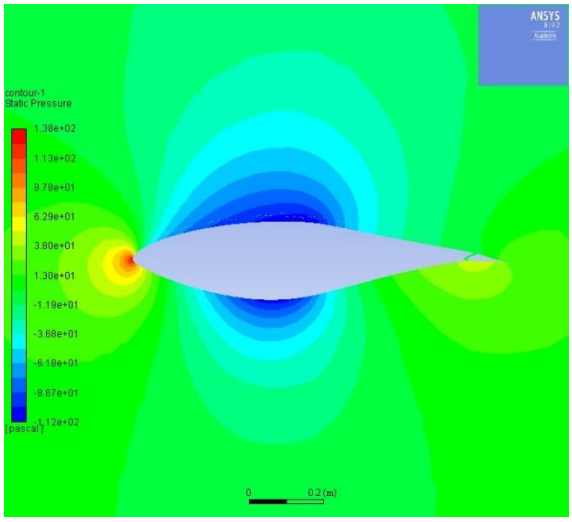

Angle of attack = 0 degree

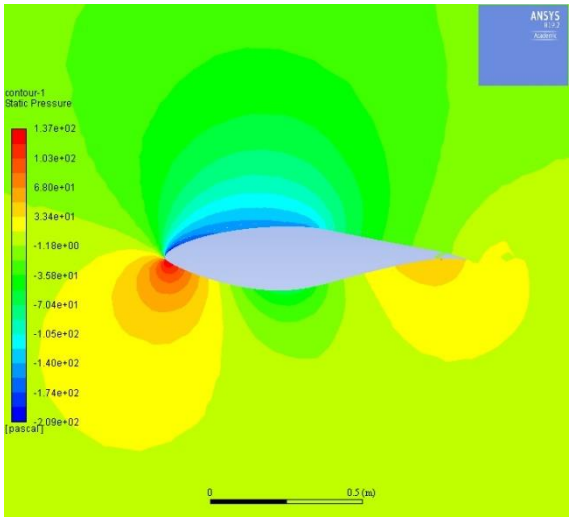

Angle of attack = 5 degrees

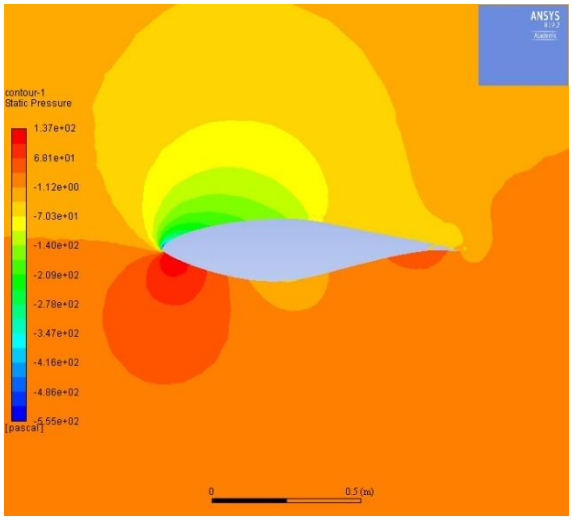

Angle of attack = 10 degrees

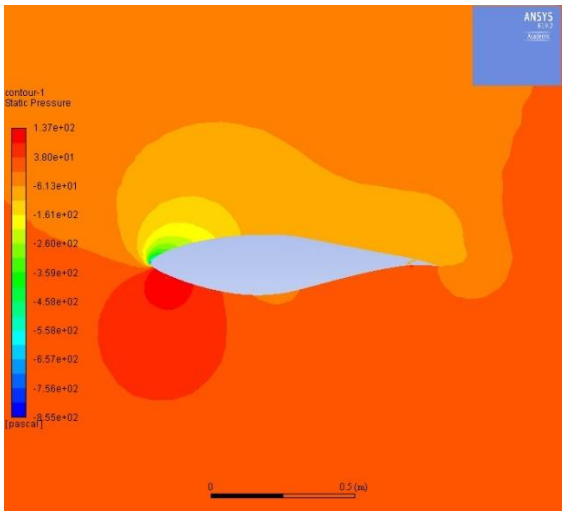

Angle of attack = 15 degrees

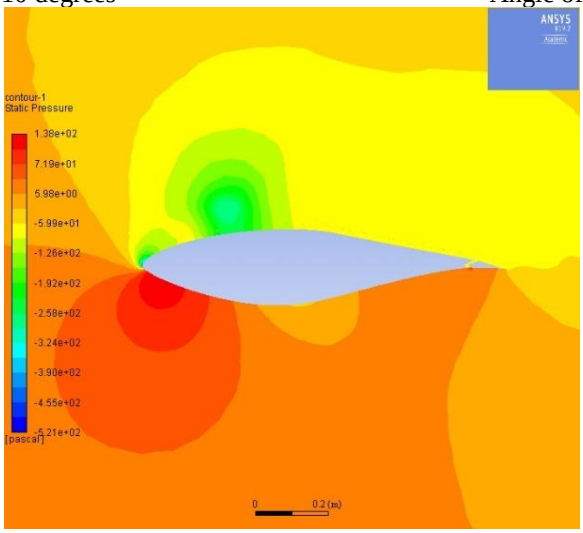

Angle of attack = 20 degrees

Figure 3.2 Pressure contours at plain flap in SA model

3.1.2 Behaviors in Shear-Stress-Transport (SST) k-ω Two-Equation Model

Fig 3.3 shows various velocity graphs exerted by SST K-ω model. When angle of attack is below 10 degrees, there is obvious velocity jump region on the lower surface and no zero-speed region occurs at trailing-edge. However, as the angle is above 10 degrees, much instable zero-speed region dominate the entire upper surface. Meanwhile, the stagnation point area and maximum velocity value also increase while AoA is increasing. Accordingly, drag force is decreasing constantly and meets the agreement of equation expression.

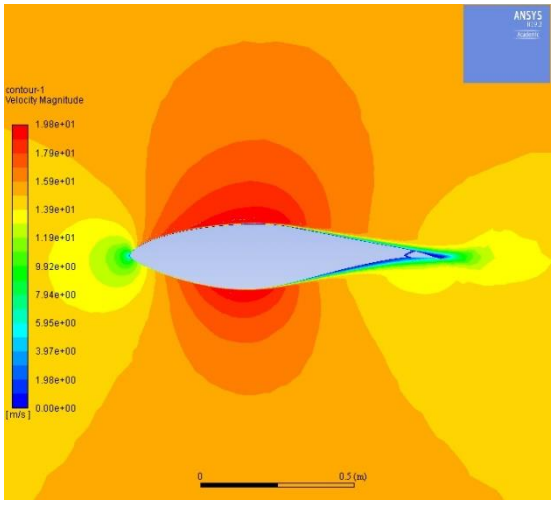

Angle of attack = 0 degree

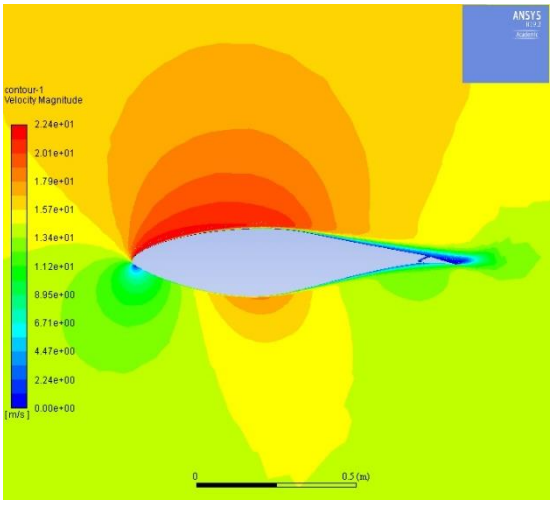

Angle of attack = 5 degrees

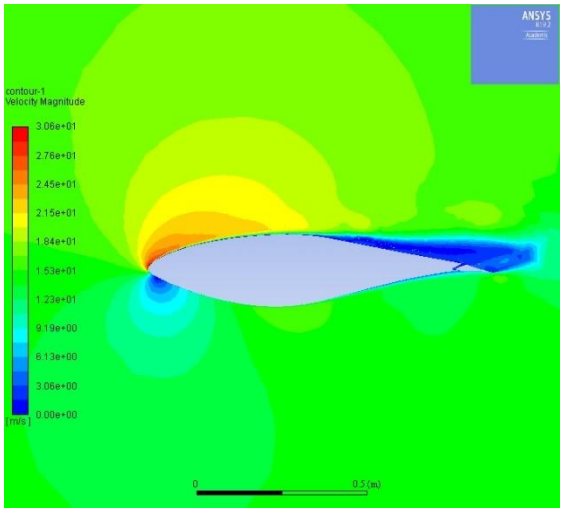

Angle of attack = 10 degrees

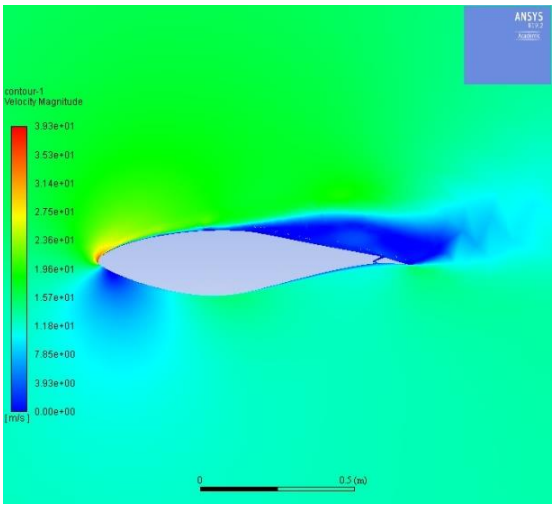

Angle of attack = 15 degrees

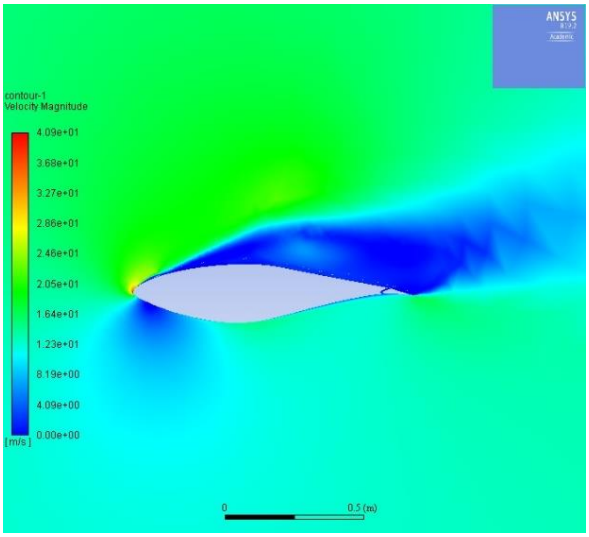

Angle of attack = 20 degrees

Figure 3.3 Velocity contours at plain flap in SST model

Five contours clearly illustrate the pressure distribution in Fig. 3.4, while the maximum pressure reading remains consistent. There is little flap effect in the first two images, however, larger pressure is generated at rear lower part of airfoil, where biggest gap happens at 10 degrees and gradually shrinks until the end. So, lift force experiences the similar trend, where several low-pressure regions on the upper surface causes suction and induce the lower lift power affect. Other than that, there is an increasing pressure distribution on the front part of airfoil as angles of attack keep climbing.

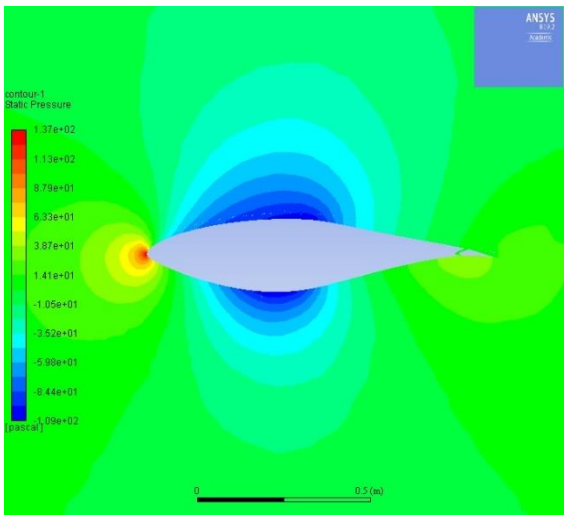

Angle of attack = 0 degree

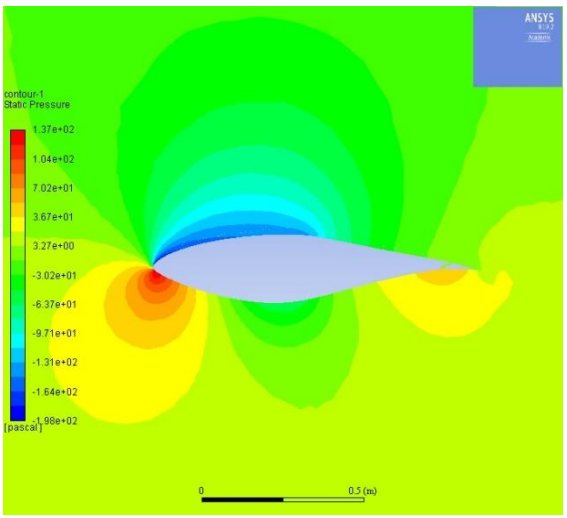

Angle of attack = 5 degrees

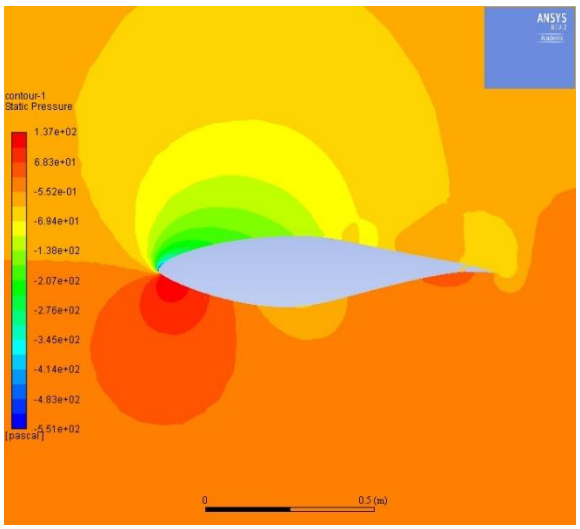

Angle of attack = 10 degrees

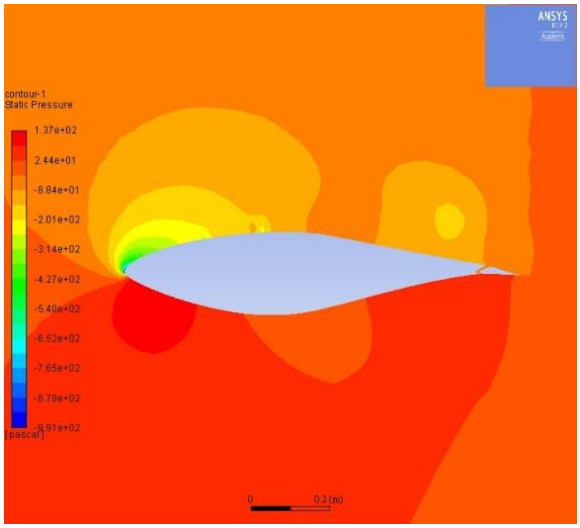

Angle of attack = 15 degrees

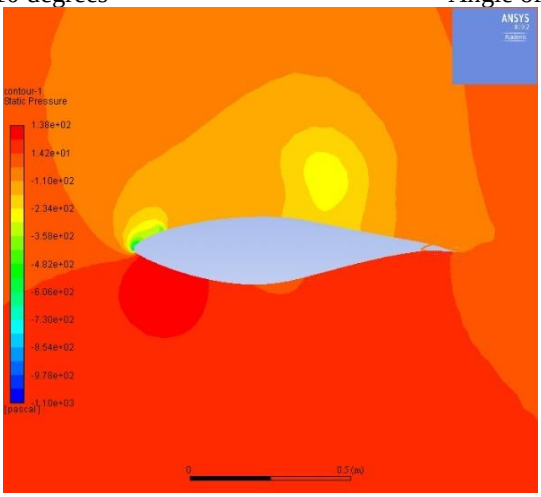

Angle of attack = 20 degrees

Figure 3.4 Pressure contours at plain flap in SST model

3.1.2 Behaviors in Wray-Agarwal (WA) One-Equation Model

Fig 3.5 shows relevant velocity contribution compared with other two models, however, there is difference: the maximum reaches the highest level and is 2.2% of greater than the previous data. Another difference is the 15-degree high speed region near the upper leading edge presents more concentrate, which casing a lower drag force and the aerodynamics performance is enhanced. Moreover, as degree increases to 20, there is no fully-covered separation region on the upper surface and this is distinct with the situations in another two models.

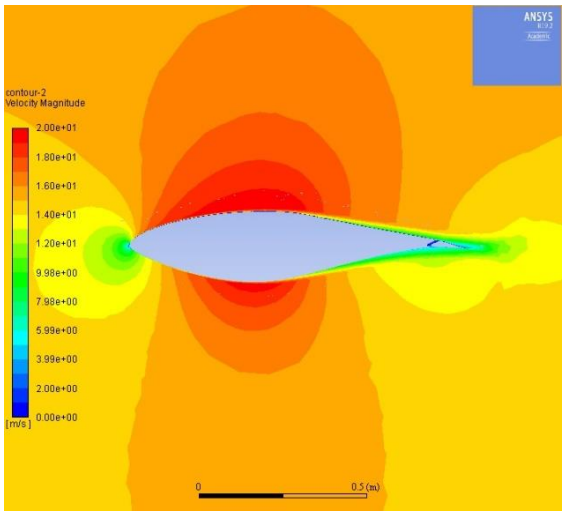

Angle of attack = 0 degree

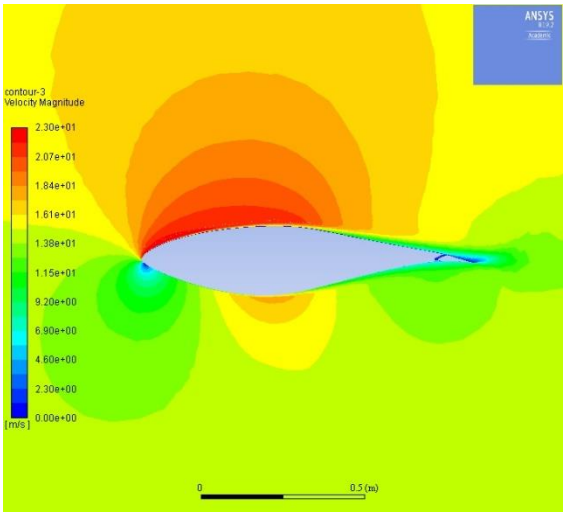

Angle of attack = 5 degrees

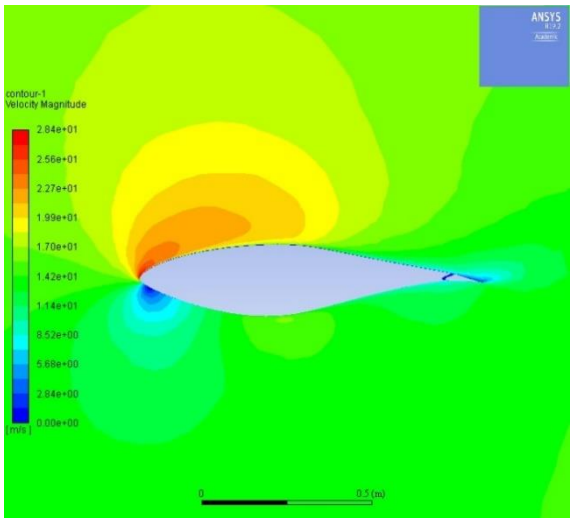

Angle of attack = 10 degrees

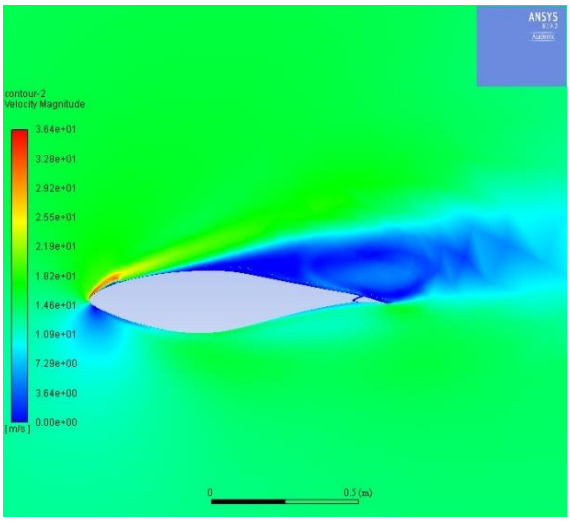

Angle of attack = 15 degrees

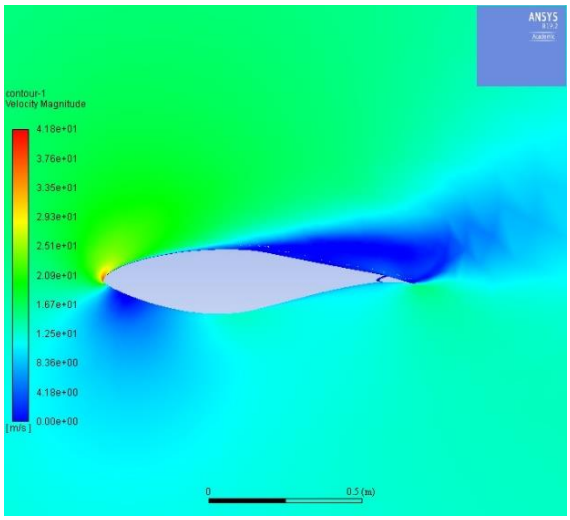

Angle of attack = 20 degrees

Figure 3.5 Velocity contours at plain flap in WA model

Fig 3.6 presents pressure contours at plain flap under WA model. One progressive observation is there is less pressure generated on the upper surface for 10 degrees case, and two suction regions are also found for 15 degrees case (one is neat the leading edge and another is at the trailing edge). They both contribute the highest lift power generation among three plain flap cases.

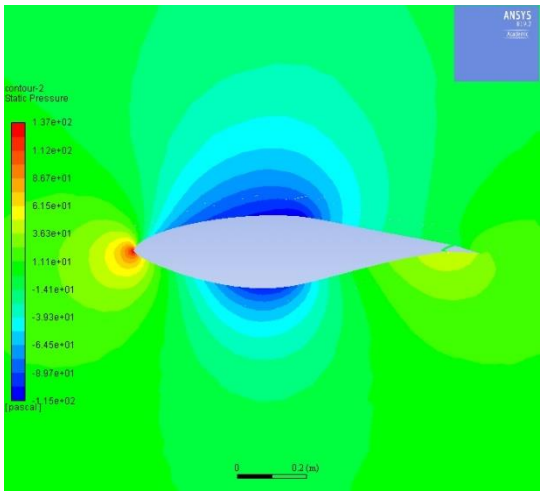

Angle of attack = 0 degrees

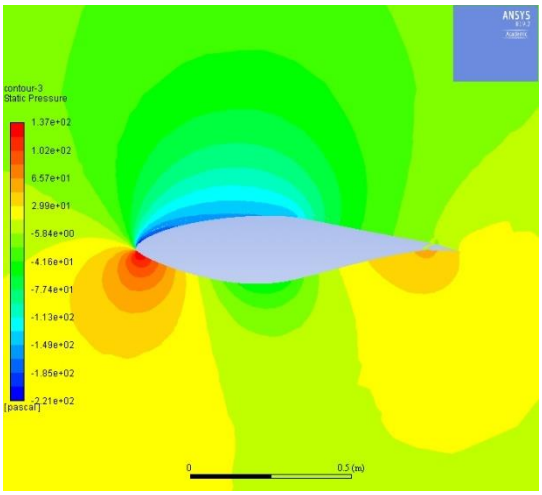

Angle of attack = 5 degrees

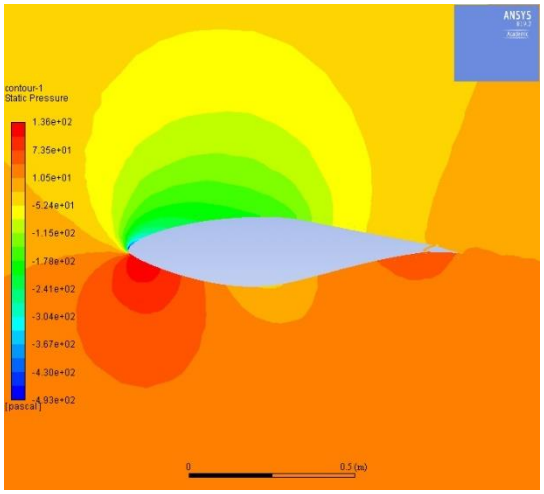

Angle of attack = 10 degrees

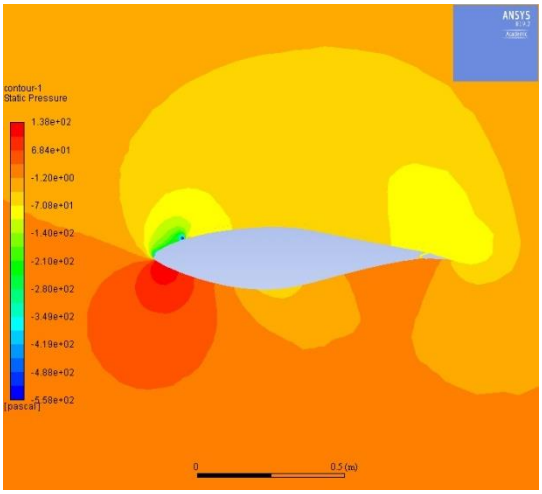

Angle of attack = 15 degrees

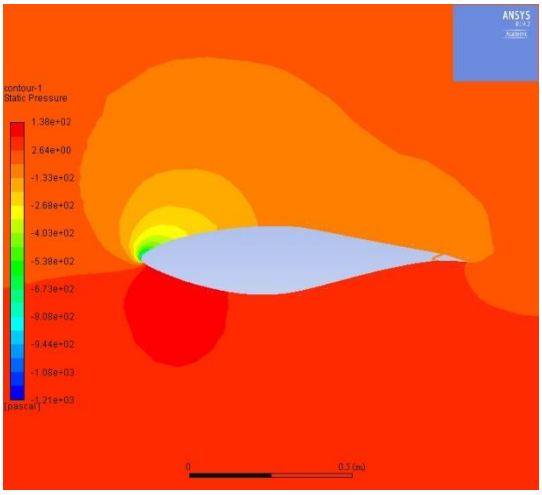

Angle of attack = 20 degrees

Figure 3.6 Pressure contours at plain flap in WA model

3.2 Lift and Drag Coefficient Analysis

The lift and drag coefficient curves for the entire S809 airfoil with plain flap are shown in Figure 3.7, 3.8. The flows at flap angles of 20 degrees are found to be unsteady, therefore the mean values are used in the lift curve and pressure coefficient plots.

In Fig 3.7, CL is increasing along with the growth of AoA, until it decreases sharply at the last position. WA model experiences the highest lift coefficient throughout the entire comparison, and the peak value occurs at 15 degrees, with a total 1.15 of reading. The maximum is followed by SA model, except a lowering outbreak at 20 degrees, which reaches 0.74 of CL. Three models both predict similar trend before angle of attack is below 10 degrees.

In Fig 3.8, CD is increasing along the x- direction, and WA model fluctuates between 15 to 20 degrees, where the lowest drag coefficient places at the last two location, coordinates the suction affect.

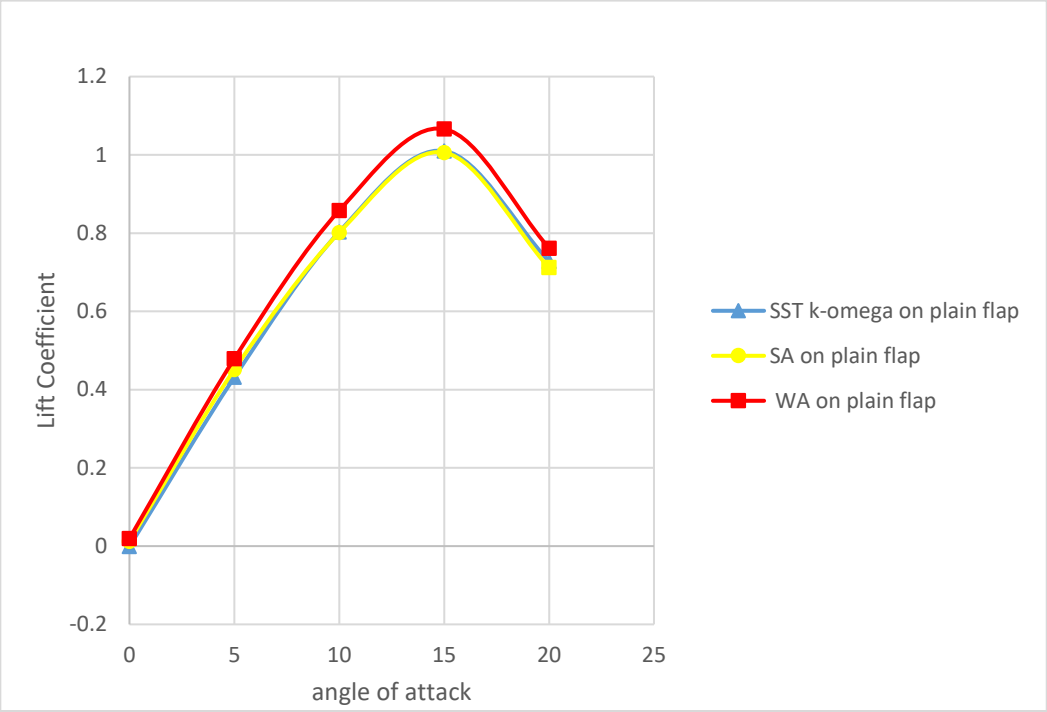

Fig 3.7 Variation in lift coefficient of S809 airfoil with plain flap

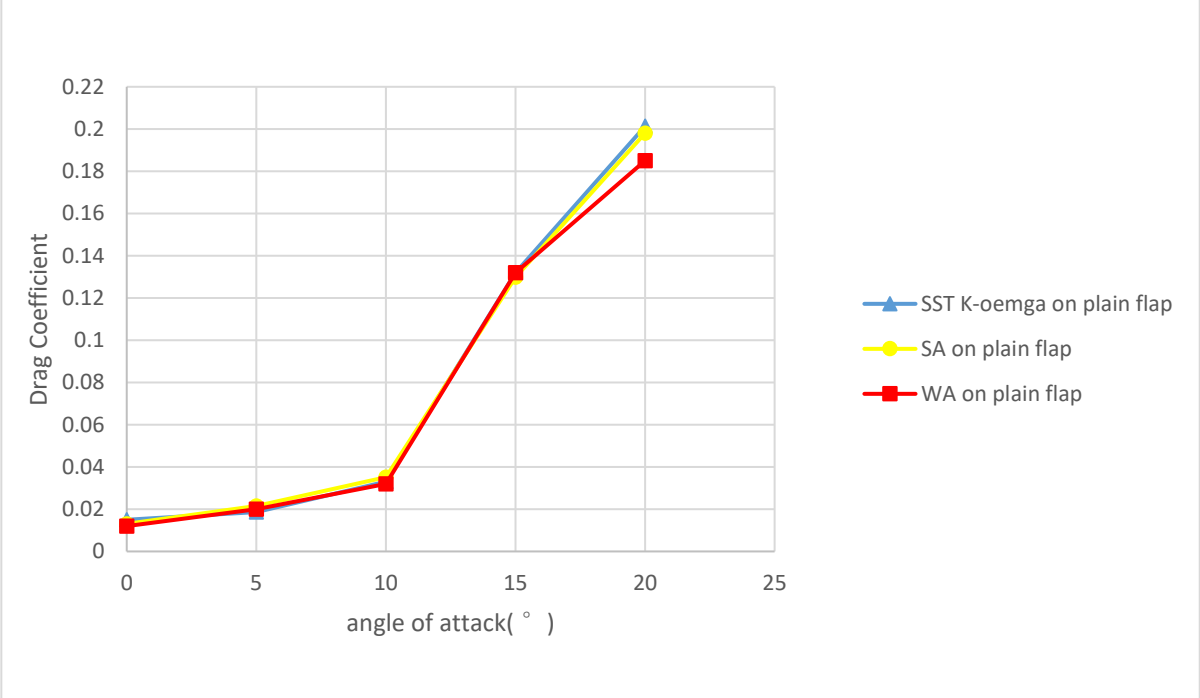

Fig 3.8 Variation in Drag coefficient of S809 airfoil with plain flap

Chapter 4: S809 Airfoil with Gurney Flap Simulation

4.1 Triangle-shaped Gurney Flap

A triangle-shaped gurney flap (GF) is selected to combine with S809 airfoil, and increases maximun lift by altering Kutta condition at the trailing-edge. The wake behind the flap is a pair of counter-rotating vortices at high angles of attack and a benefit in overall lift-to-drag ratio is also possible if the flap is tailored appropriately. Fig 4.1 shows the geometric configuration of entire form shape.

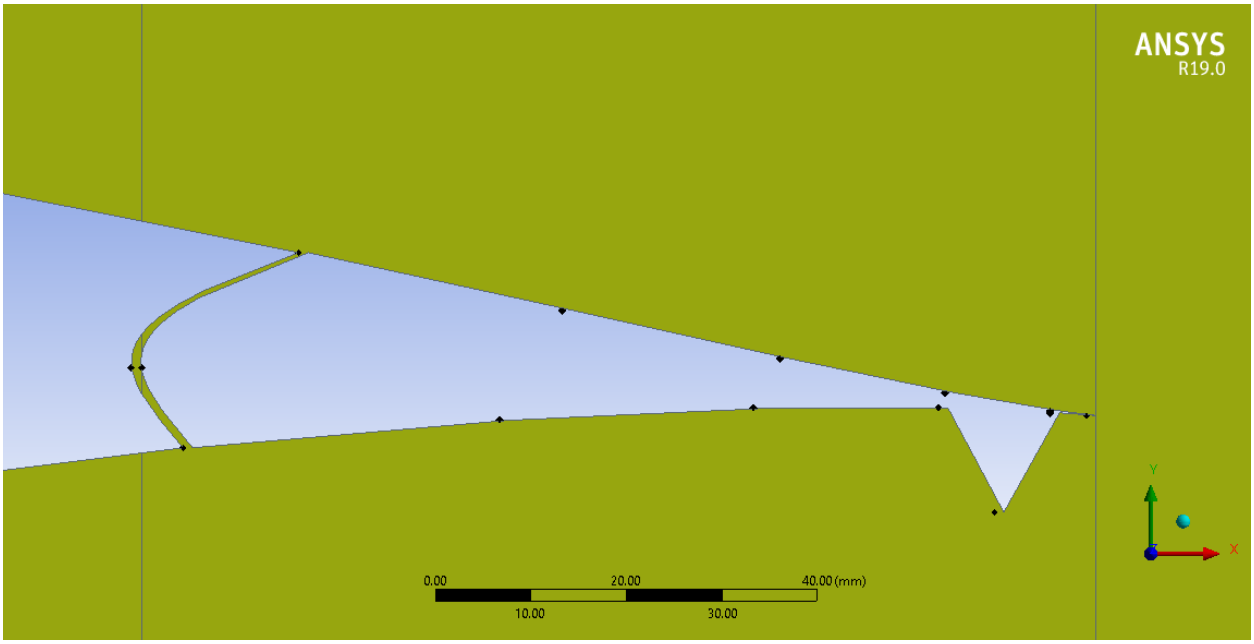

Fig 4.1 Schematic of S809 airfoil with triangle-shaped gurney flap

4.2 Flow Field Information and Discussion

4.2.1 Behaviors in Spalart-Allmaras (SA) One-Equation Model

Figure 4.2 shows the velocity contours around airfoil at different angles of attack. The velocity on the upper surface becomes smaller as the angle increases but it is below 15 degrees. Thus, the lift coefficient increases when angle of attack is below 15 degrees. For angle is greater than 15 degrees,

the velocity on the upper surface decreases at the angle becomes larger. This makes the pressure distribution on the upper surface becomes larger, which weakens the suction on the upper surface. Thus, the lift coefficient decreases when angle is greater than 15 degrees. Moreever, there are two velocity jump regions at the leading-edge, when the angel of attack is over 10 degrees. More concentrate high-speed scale places at upper and diffused low-speed scale is at the bottom.

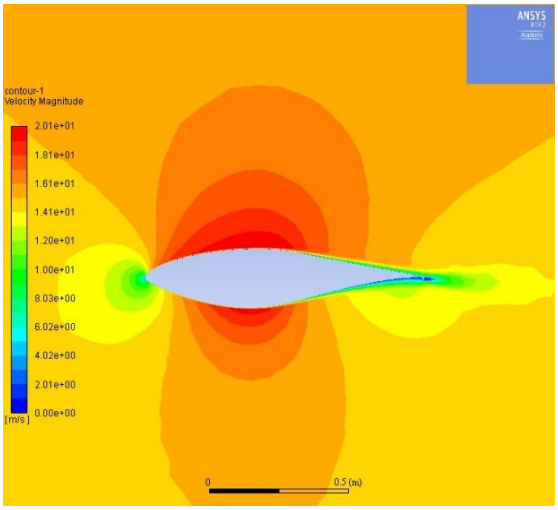

Angle of attack = 0 degree

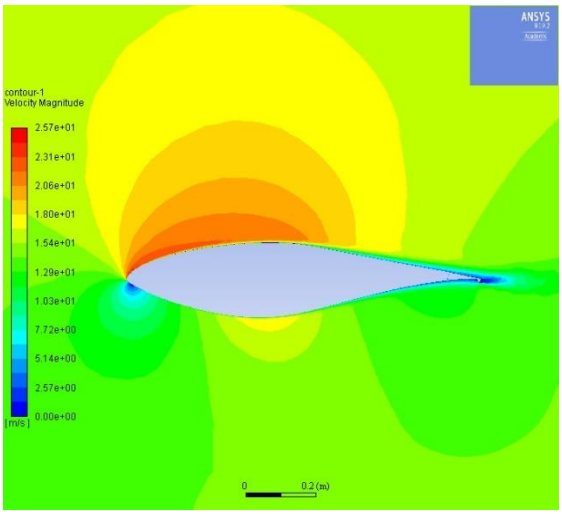

Angle of attack = 5 degrees

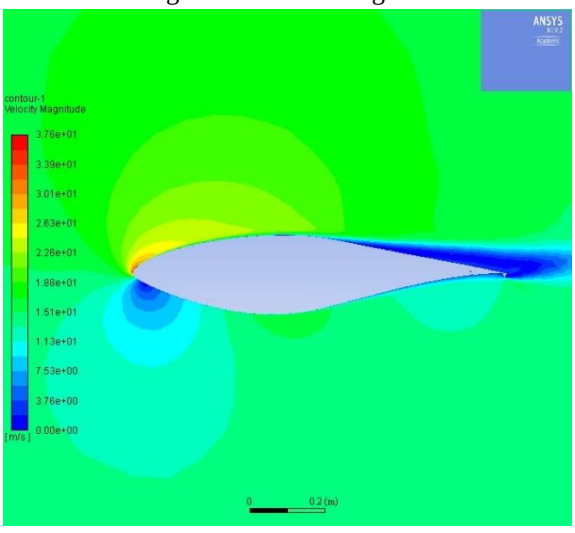

Angle of attack = 10 degrees

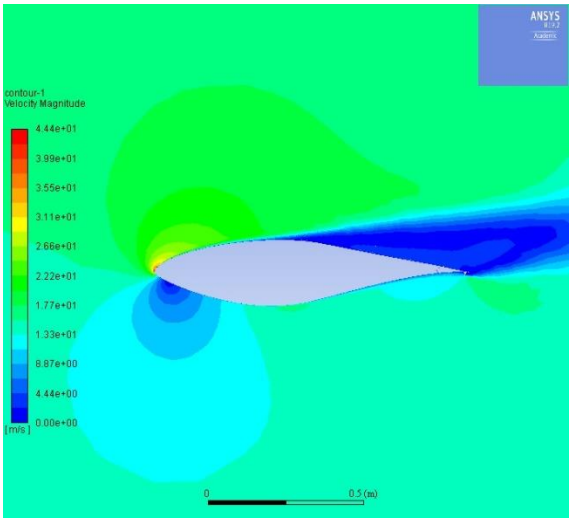

Angle of attack = 15 degrees

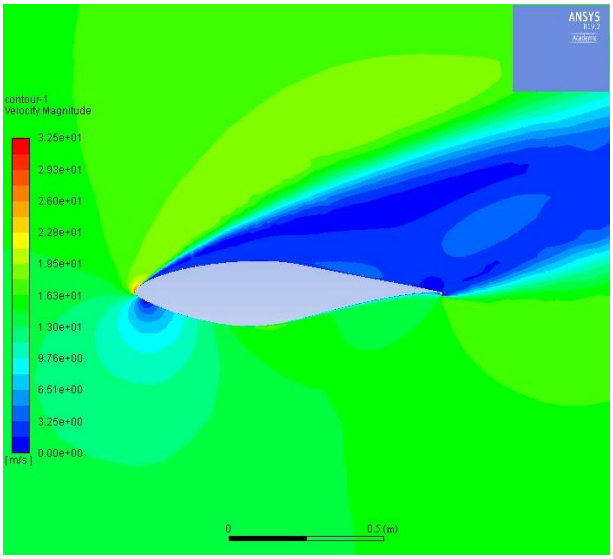

Angle of attack = 20 degrees

Figure 4.2 Velocity contours at Gurney flap in SA model

Figure 4.3 shows the pressure coefficient contours around the airfoil with at different angles of attack. When angle is over 10 degrees, there is high pressure region generated on the lower surface of the airfoil near the leading edge and the trailing edge due to the presence of gurney flap. And the suction on the upper surface also increases. When angle is less than 10 degrees, the high-pressure region on the lower surface near the leading and trailing edge decreases, and the high-pressure region near the trailing edge almost disappears. When the angle of attack is 15 degrees,

there is greatest pressure generated at the lower surface, which gives a highest lift coefficient.

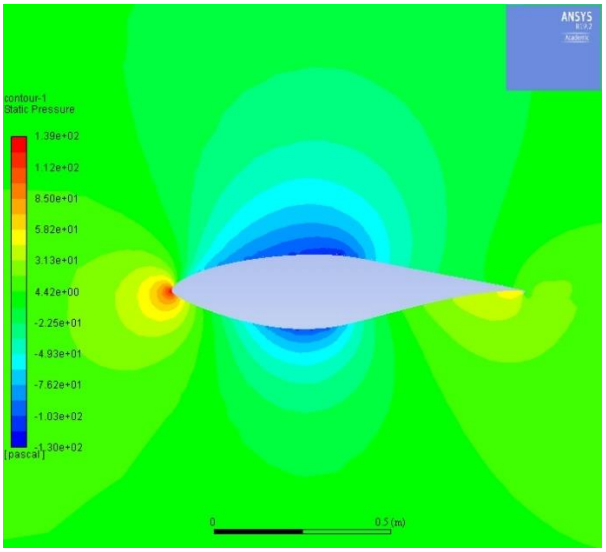

Angle of attack = 0 degree

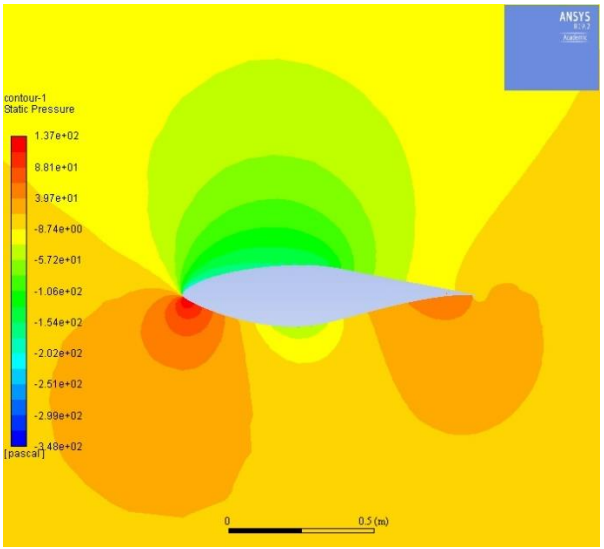

Angle of attack = 5 degrees

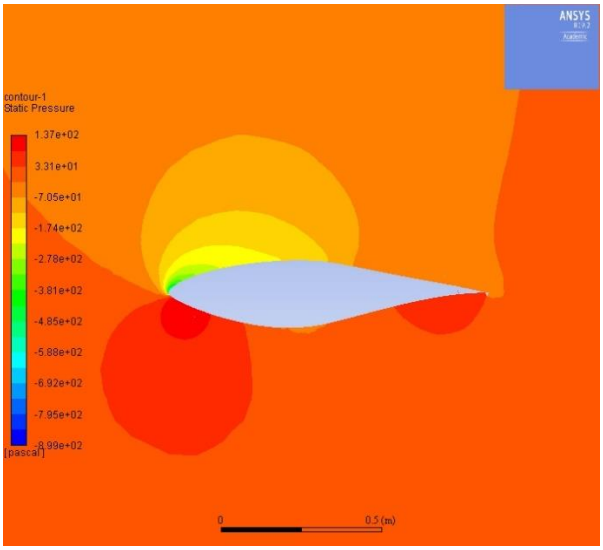

Angle of attack = 10 degrees

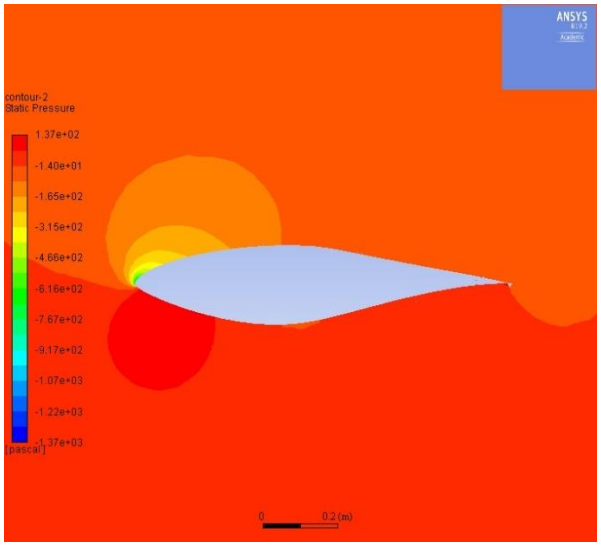

Angle of attack = 15 degrees

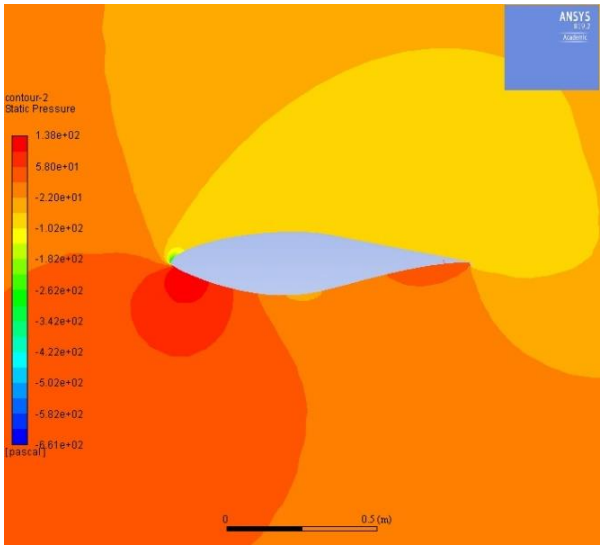

Angle of attack = 20 degrees

Figure 4.3 Pressure contours at Gurney flap in SA model

4.2.2 Behaviors in Shear-Stress-Transport (SST) k-ω Two-Equation Model

Figure 4.4 show the velocity distribution contours around the airfoil with Triangle-shaped Gurney flap in SST k-ω model. The velocity on the upper surface becomes smaller as the angles of attack increase. This decreases the less pressure distribution on the upper surface, which result in more suction on the upper surface. Thus, the lift coefficient increases when the angle is below 15 degrees. For angle greater than 15 degrees, the velocity on the upper surface decreases becomes larger. This results in the pressure distribution on the upper surface becoming larger, which weakens the suction on the upper surface. Thus, the lift coefficient decreases when angle is greater than 15 degrees.

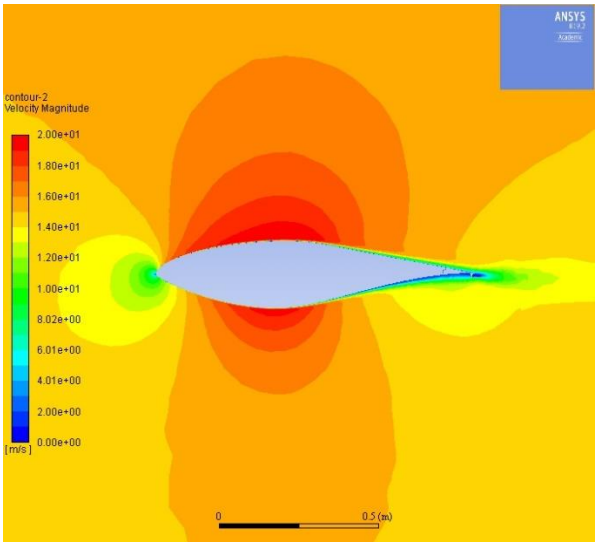

Angle of attack = 0 degrees

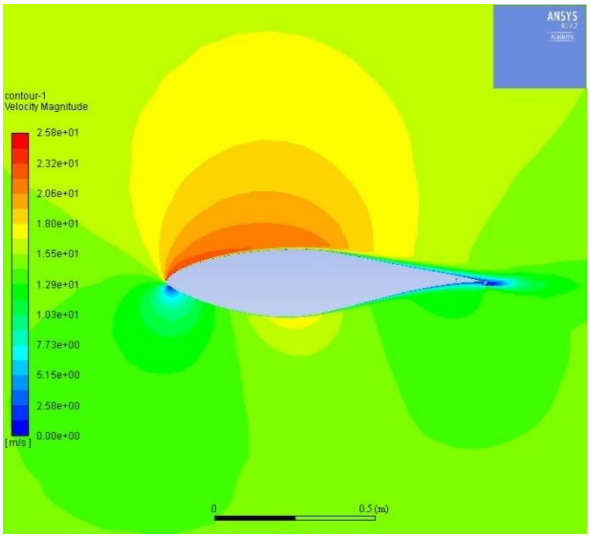

Angle of attack = 5 degrees

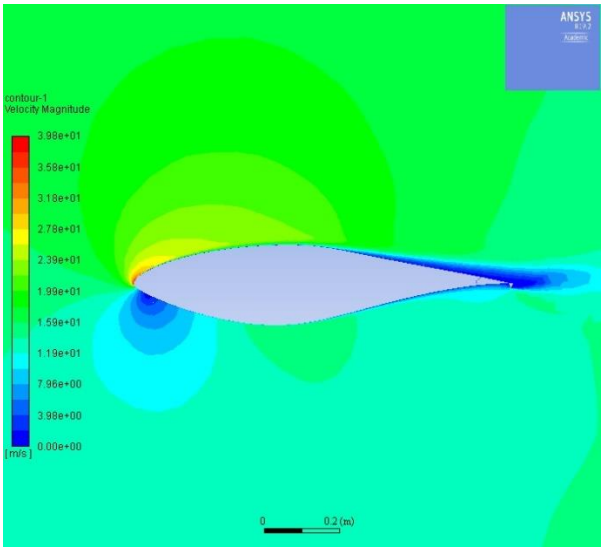

Angle of attack =10 degrees

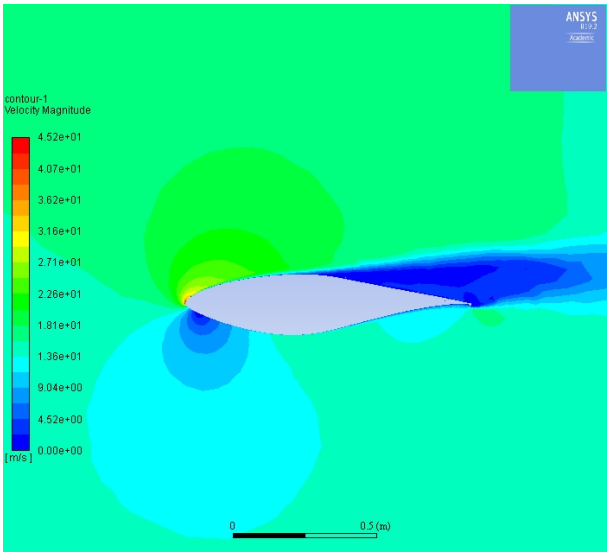

Angle of attack = 15 degrees

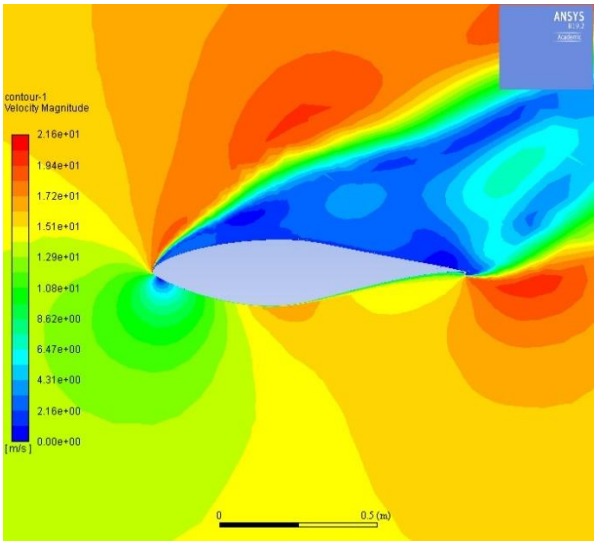

Angle of attack = 20 degrees

Figure 4.4 Velocity contours at Gurney flap in SST model

Figure 4.5 shows the pressure coefficient contours of the S809 airfoil with different angles of attack in SST k-ω model. When angle is between 10 to 15 degrees, there is high pressure region generated on the lower surface near the leading edge and the trailing edge. When angle is greater than 15 degrees, the high-pressure region on the lower surface near the leading edge and the trailing edge decreases, and the high-pressure region moves to the trailing edge and a low-pressure region occurs at rear part of the flap.

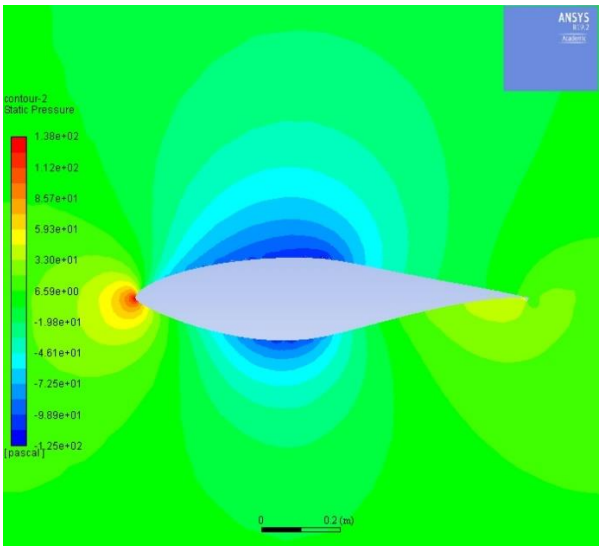

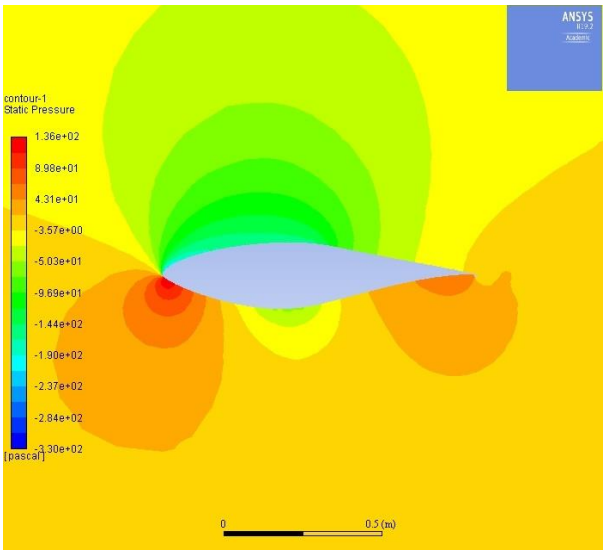

Angle of attack = 0 degrees

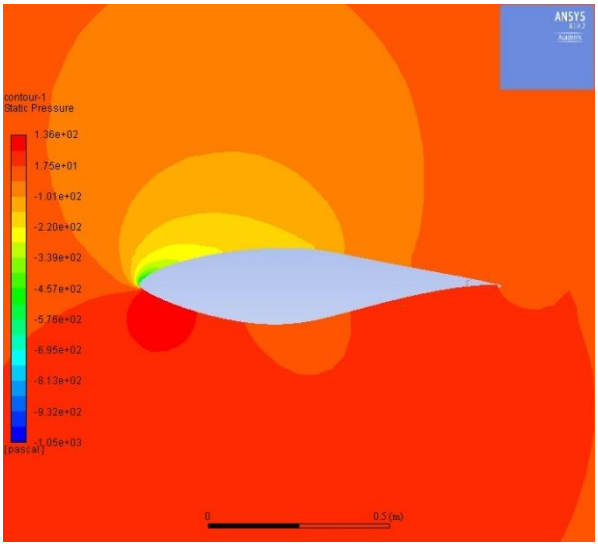

Angle of attack = 5 degrees

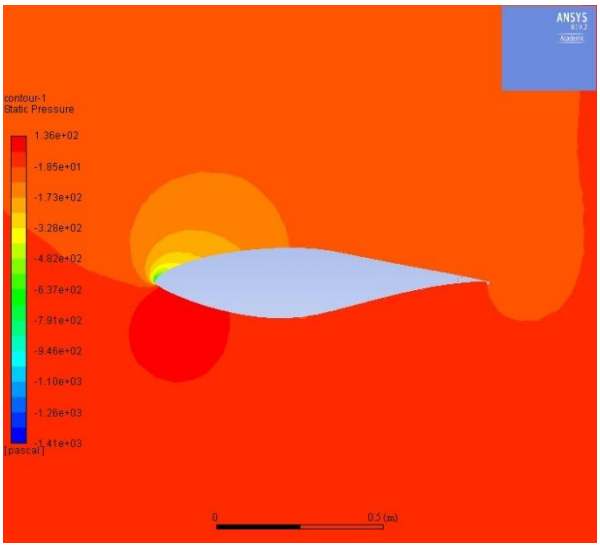

Angle of attack = 10 degrees

Angle of attack = 15 degrees

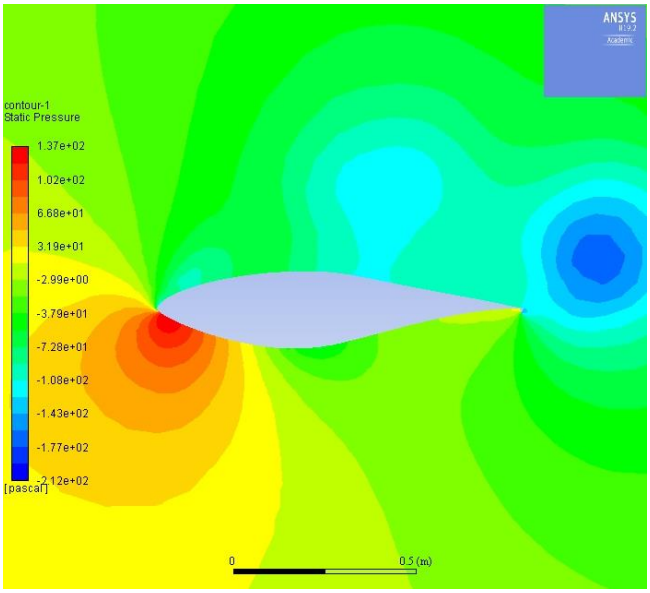

Angle of attack = 20 degrees

Figure 4.5 Pressure contours at Gurney flap in SST model

4.2.3 Behaviors in Wray-Agarwal (WA) One-Equation Model

Figure 4.6 shows the velocity contours around airfoil with Gurney flap for various angles of attack. It can be seen that the WA model helps augmenting maximum lift force, and the boundary layer is steady and stable when angle is lower than 10 degrees. The upper surface pressure coefficient

decreases and the lift increases. When angle becomes greater than 15 degrees, there is separation on the upper surface of the flap which leads to decrease in lift.

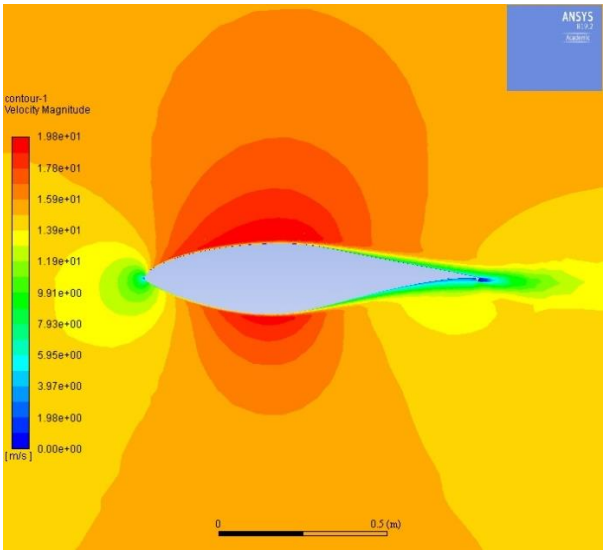

Angle of attack = 0 degree

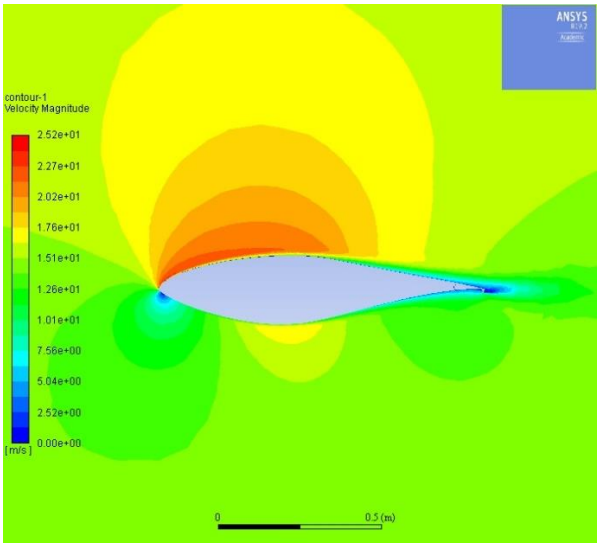

Angle of attack = 5 degrees

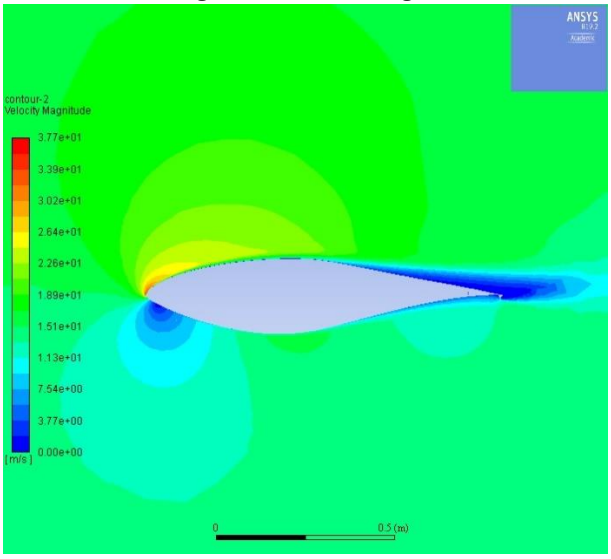

Angle of attack = 10 degrees

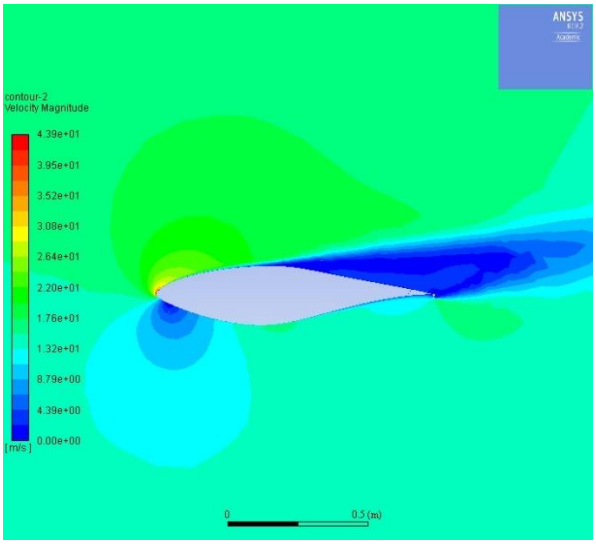

Angle of attack = 15 degrees

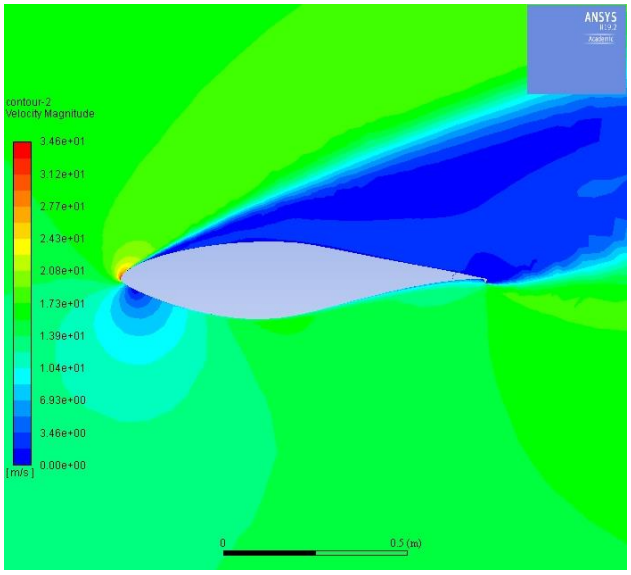

Angle of attack = 20 degrees

Figure 4.6 Velocity contours at Gurney flap in WA model

Figure 4.7 shows the pressure coefficient contours around the airfoil in WA model. When the Gurney flap is applied on the airfoil in this case, the upper surface suction increases compared to the airfoil without prescribed flap especially for angles greater than 15 degrees. And less pressure generates at the trailing edge because of the effect of the flap. For angle 0 degrees and 5degrees, the suction on the upper surface is similar to the data displayed in other two models.

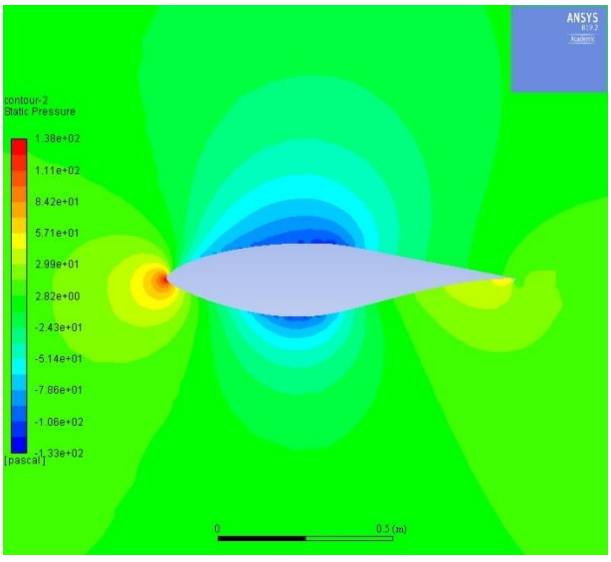

Angle of attack = 0 degrees

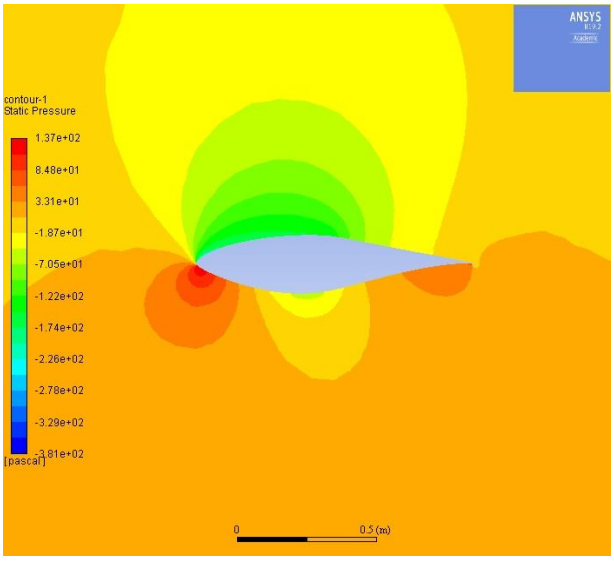

Angle of attack = 5 degrees

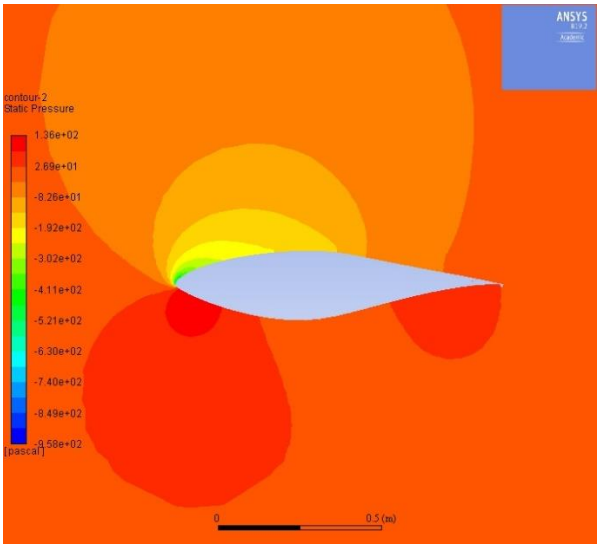

Angle of attack = 10 degrees

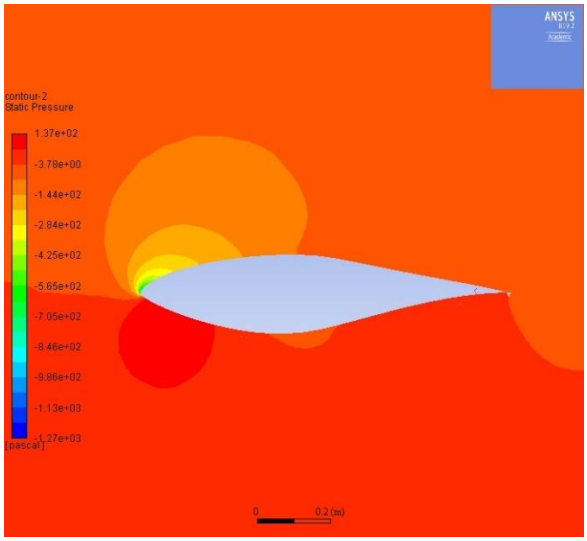

Angle of attack = 15 degrees

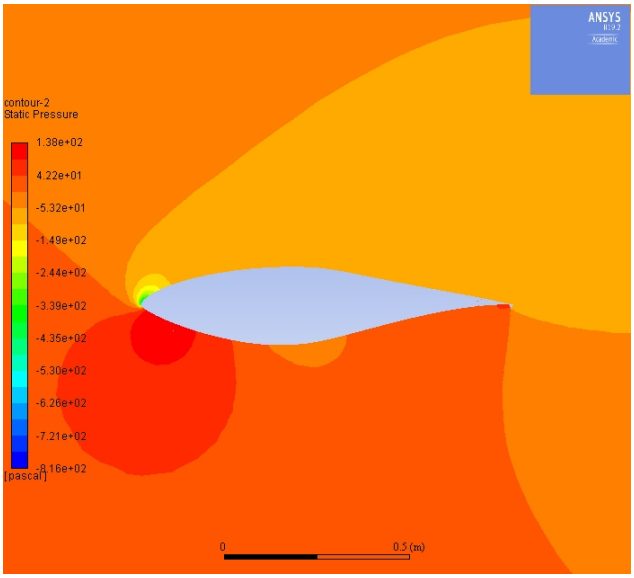

Angle of attack = 20 degrees

Figure 4.7 Pressure contours at Gurney flap in WA model

4.3 Lift and Drag Coefficient Analysis

In Fig 4.8 and 4.9, lift and drag coefficient plots with triangle-shaped Gurney Flap are presented in three turbulence models. WA model curve experiences a gradual increase at the first three degree and reaches maximum CL of 1.17 at 15 degrees, then decreased by 33%. SA and SST K-omega model curves exerts analogous trend; however, the entire data is below the first model curve. For the drag coefficient graph, the three models ascend from 0 to 20 degrees, there is a sharp augment

at 15 degrees and little fluctuation at 20 degrees. WA model also gains a greatest drag coefficient when angle of attack is 20 degrees.

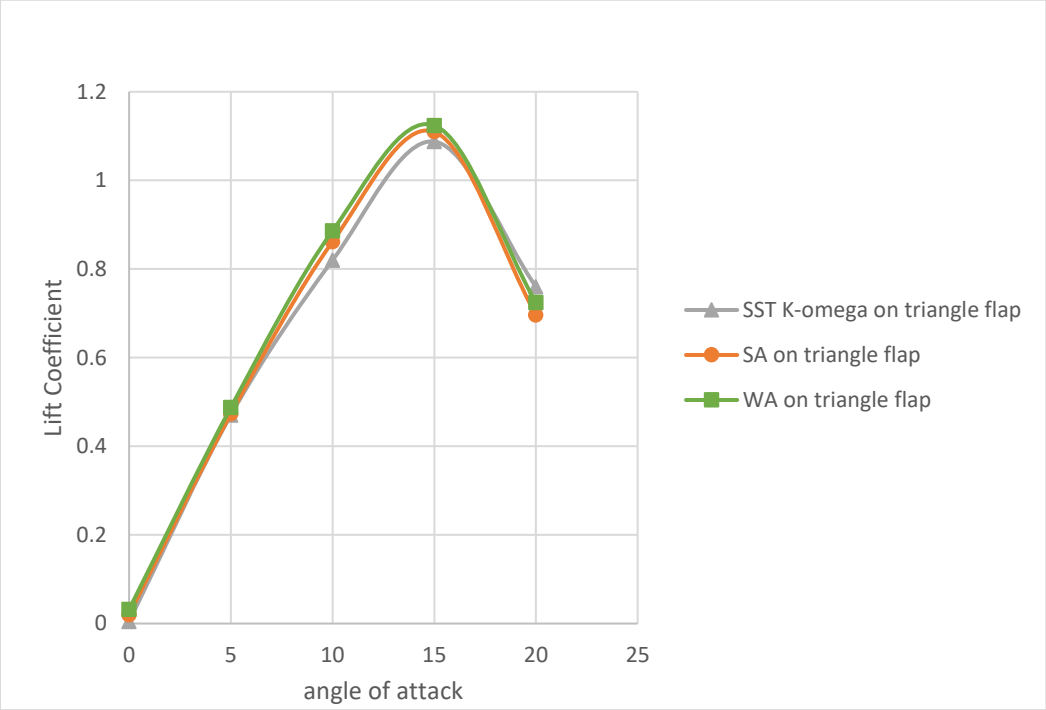

Fig 4.8 Variation in lift coefficient of S809 airfoil with Triangle Gurney Flap

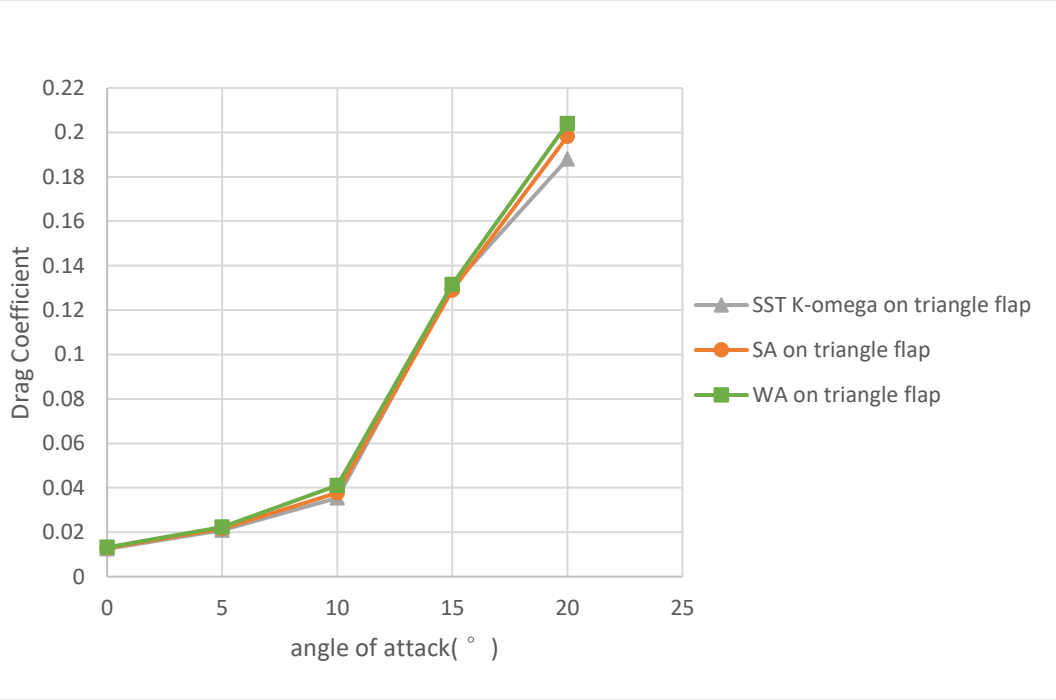

Fig 4.9 Variation in drag coefficient of S809 airfoil with Triangle Gurney Flap

The performance of aerodynamics of the plain flap can also be investigated by varying flap deflection angles, ranging from -5 to 10 degrees, solved by SST *k*-ω model. On the basis of gap difference optimization from previous paper, distance is set to 1mm. The angle of attack is also chosen from 0, 2.5, and 5 degrees, and lift coefficient is plotted and compared in Fig 4.10 with installin plain and gurney flap at the trailing-edge. When angle of attack is 0 degree, two lines start at similar lift coefficient, and then experience a near-linearly ascend respectively. It is clearly to find Cl increases along with an improve flap deflection angle. Besides, airfoil with gurney flap obtains a higher lift coefficient compared with the value with plain-flap airfoil, and the biggest difference occurs when flap deflection angle is 8 degree under a 5-degree angle of attack. Therefore, the trailing-edge gurney flap can effectively improve Cl for a proposed airfoil at same angle of attack.

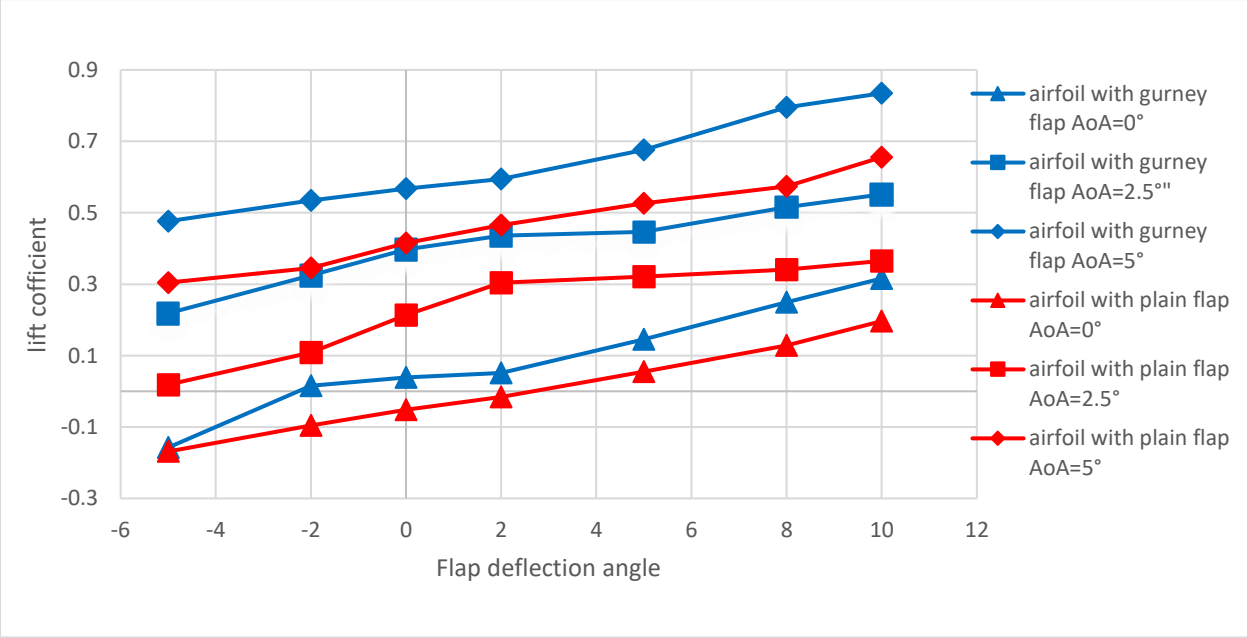

Fig 4.10 Lift coefficient vs flap deflection angle

When the angle of attack is small, the lift-to-drag ratio increases as flap deflection angle increases in Fig 4.11; however, when the angle of attack is greater than 2.5 degrees , the lift-to-drag coefficient experience a dramatic growth in large flap deflection angles, and follow a steady

fluctuation with a flap deflection angle of 2 to 5 degrees. There is a slight rise and large drop when angles continue to improve, where the greatest ratio occurs angle is set to 8 degrees. Accordingly, lift-to-drag ratio can be obviously improved with the presence of gurney flap at the trailing-edge angle, and the value is largely affected when angle of attack is increasing.

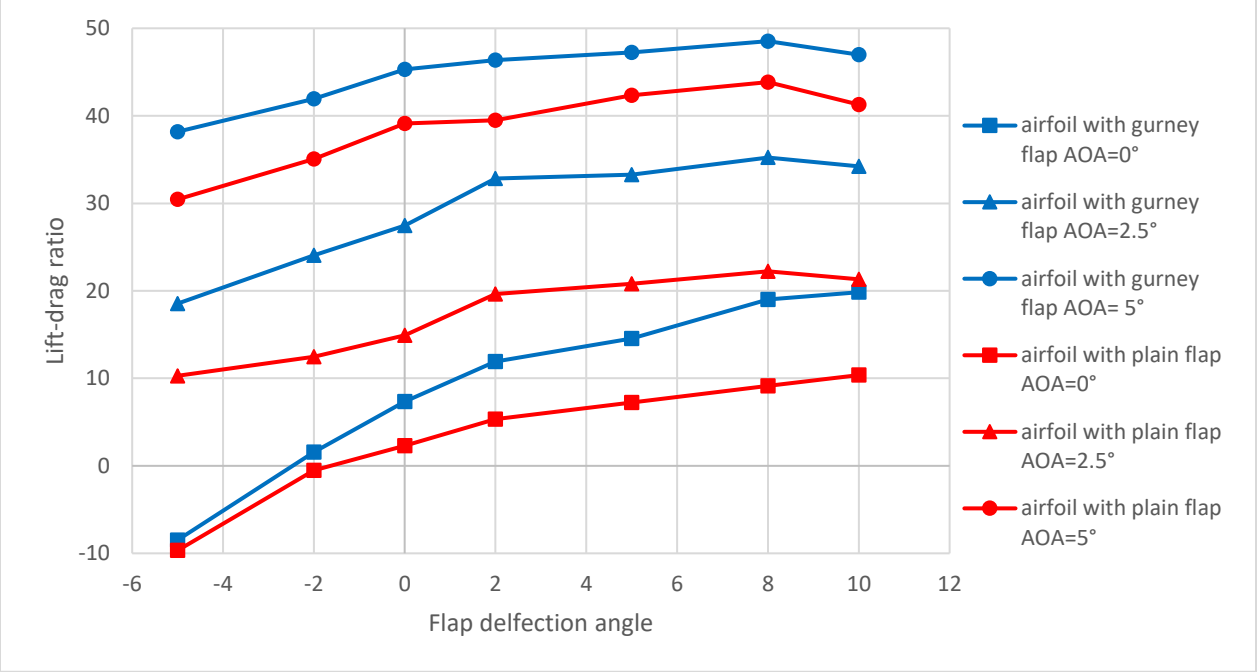

Fig. 4.11 Lift-to-drag coefficient vs. flap deflection angle

4.4 Pressure Coefficient Analysis

Fig 4.12 presents pressure coefficient distributions of the airfoil with proposed flaps with different flap deflection angles. There is big pressure difference at x=0.35m, where the difference decreases when flap deflection angle is smaller(when flap angle is set to 5 degrees, there is little pressure difference influence at x=0.35m). And CP is decreasing obviously at lower leading edge surface when flap deflection angle is increasing. Besides, the plain flap with bigger deflection angle also affects a larger pressre coefficient difference generation.

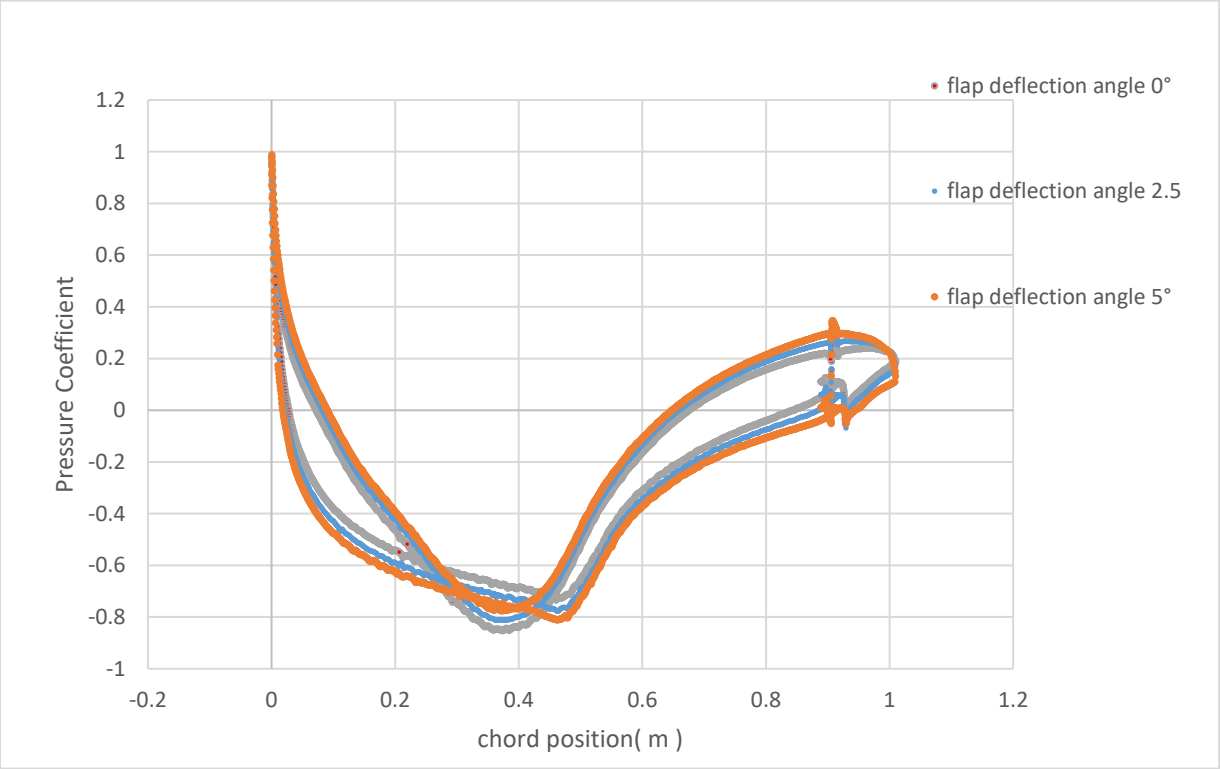

Fig. 4.12 Pressure coefficient distributions with different flap deflection angles

Chapter 5: Comparison and Conclusion

Fig 5.1 and 5.2 show the lift and drag coefficient variation of three models between two types of flap. WA model always obtains the highest CL at 15 degrees of angel of attack under with same flap, which much lift force is generated due to affect of the prescribed one equation turbulance model UDF file. The biggest CL difference also occurs at maximum reading , the value of WA on triangle-shaped Gurney Flap is increased by 14.5% compared to SA model on plain flap. When the angle of attack is below 10 degrees, little fluctuation dominates in the flowfield.

The drag coefficient experiences a gradual increase at first two degrees, and then leads a tiny variation, where WA model with traingle flap reaches the greatest drag coefficient (0.042) at 10

degrees and WA model with plain flap reaches the lowest of 0.031. Next, a huge rise comes to approximately 0.13, while there is bo obvious difference at this point, and then it is followed by several diffused ascend ,contributing the highest CD at 20 degrees by WA triangle flap model in the entire chart.

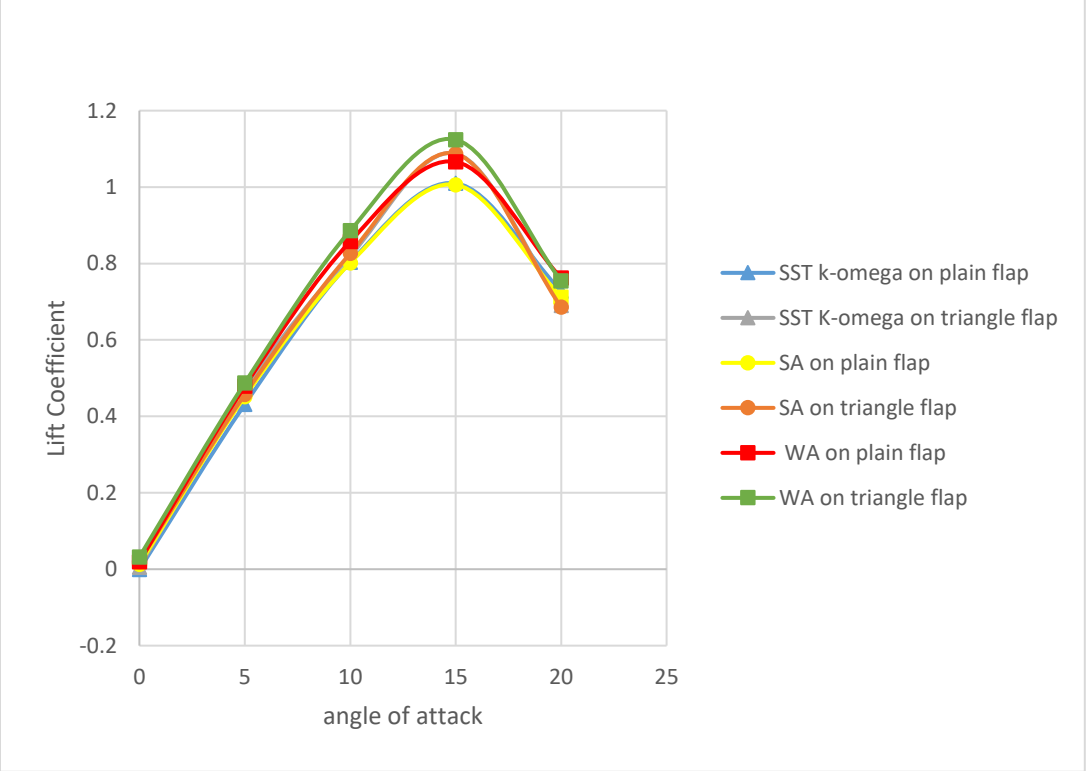

Fig 5.1 Variation in Lift coefficient of S809 airfoil with Triangle Gurney Flap and Plain flap

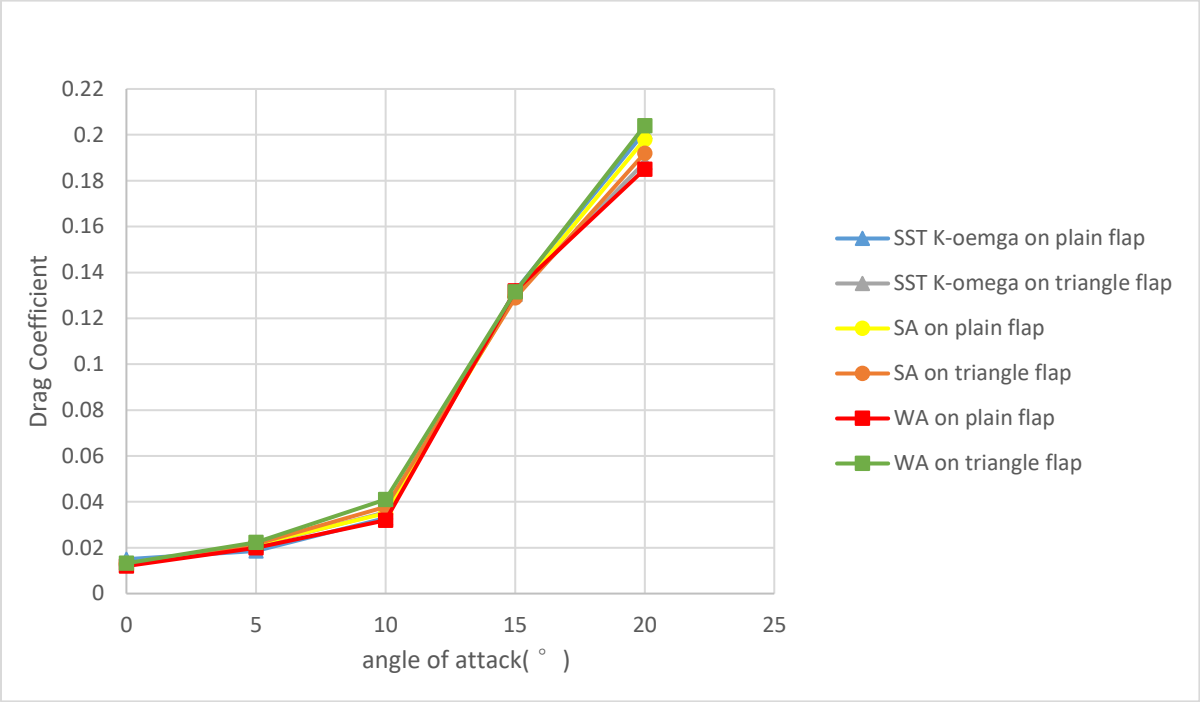

Fig 5.2 Variation in Drag coefficient of S809 airfoil with Triangle Gurney Flap and Plain flap

In this defense, a proposed trailing-edge flap is designed by adding a rotatable flap to the NREL's S809 airfoil trailing-edge flap(controlled by a variable pitch controller), the entire aerodynamics calculation and performance are carried out by ANSYS FLUENT 19.2. The results are: all turbulence models give similar results and compare well with experimental data in non-stall regime. the trailing-edge flap can significantly improve the lift coefficient, lift-to-drag coefficient and the drag coefficient is also ascended inevitably; For the WA model, more lift and drag coefficient is generated compared with other two models pressure coefficient difference and lift coefficient become larger when flap deflection angle increases. Morever, triangle-shape Gurney Flap can enhance greater Cl.

In the future, an air-sand particle two phase flow can be further analyzed in the study, and Microtab and Gurney Flap blade design with active control approach can also be investigated, in order to reduce maximum drag coefficient

References

[1]. U.S. Department of Energy Office of Scientific and Technical Information https://www.energy.gov/sites/prod/files/2018/08/f54/2017_wind_technologies_market_report_8.15.18.v2.pdf

[2]. T. K. Barlas, G. A. M. van Kuik. Review of state of the art in smart rotor control research for wind turbines. Progress in Aerospace Sciences, 2010(46): 1-27.

[3]. Lee SG, Park SJ, Lee KS, Chung C. Performance prediction of NREL Phase VI blade adopting blunt trailing edge airfoil. Energy, 2012, 47(1): 47-61.

[4]. Liu ZY, Wang XD, Kang S. Stochastic performance evaluation of horizontal axis wind turbine blades using nondeterministic CFD simulations. Energy, 2014. 73: 126-136.

[5]. Douvi, D.C.; Margaris, D.P. Comparison Between New and Existing Turbulence Models for Numerical Simulation of the Flow Over NACA 0012 and S809 Airfoils for Two Reynolds Numbers. In Proceedings of the 6th International Conference on "Experiments/Process/System Modelling/Simulation/Optimization",

[6]. CFD Calculations of S809 Aerodynamic Characteristics

[7]. Barlas T, Lackner M. Smart rotor blade technology applied to the Upwind reference turbine. Proceedings of the IEA topical expert meeting on the application of smart structures for large wind turbine rotor blades, Sandia National Labs, Albuquerque, USA May 2008.

[8]. Design optimization of a wind turbine blade to reduce the fluctuating unsteady aerodynamic load in turbulent wind†

[9]. Menter, F.R. Two-Equation Eddy-Viscosity Turbulence Models for Engineering Applications. AIAA J. 1994, 32, 1598–1605. [CrossRef]

[10]. Wray, T. J., and Agarwal, R. K., "A New Low Reynolds Number One Equation Turbulence Model Based on a k-ω Closure." AIAA Journal, Vol. 58, No. 8, pp. 2216-2227.

Curriculum Vita

Heyou Tan

Degrees M.S. Mechanical Engineering, May 2020
B.S. Marine Engineering, July 2017

May,2020